This is a preprint, the final version is subject to change, of the American Mineralogist (MSA)
Cite as Authors (Year) Title. American Mineralogist, in press.
(DOI will not work until issue is live.) DOI: http://dx.doi.org/10.2138/am-2017-5763

Revision 1

Nickel variability in Hawaiian olivine: Evaluating the relative contributions from mantle and crustal processes

Kendra J. Lynn*, Thomas Shea, and Michael O. Garcia

*kjlynn@hawaii.edu

Department of Geology and Geophysics, University of Hawai‘i, Honolulu, HI 96822, USA

ABSTRACT

Olivine in Hawaiian tholeiitic lavas have high NiO at given forsterite (Fo) contents (e.g. 0.25-0.60 wt % at Fo_{88}) compared to MORB (e.g. 0.10-0.28 wt% at Fo_{88}). This difference is commonly related to source variables such as depth and temperature of melting, and/or lithology. Hawaiian olivine NiO contents are also highly variable and can range from 0.25-0.60 wt% at a given Fo. Here we examine the effects of crustal processes (fractional crystallization, magma mixing, diffusive re-equilibration) on the Ni content in olivine from Hawaiian basalts. Olivine compositions for five major Hawaiian volcanoes can be subdivided at $\geq Fo_{88}$ into high-Ni (0.25-0.60 wt% NiO; Ko‘olau, Mauna Loa, and Mauna Kea) and low-Ni (0.25-0.45 wt% NiO; Kīlauea and Lō‘ihi), groups that are unrelated to major isotopic trends (e.g. Loa and Kea). Within each group, individual volcanoes show up to 2.5x variation in olivine NiO contents at a given Fo. Whole-rock Ni contents from Ko‘olau, Mauna Loa, Mauna Kea, and Kīlauea lavas overlap significantly and do not correlate with differences in olivine NiO contents. However, inter-volcano variations in parental melt polymerization (NBO/T) and nickel partition coefficients ($D_{Ni}^{ol/melt}$), caused by variable melt SiO_2, correlate with observed differences in olivine NiO at Fo_{90}, indicating that an olivine-free source lithology does not produce the inter-volcano groups. Additionally, large intra-volcano variations in olivine NiO can occur with minimal variation in lava SiO_2 and NBO/T. Minor variations in parental melt NiO contents (0.09-0.11 wt%) account

for the observed range of NiO in ≥ Fo_{88} olivine. High precision electron microprobe analyses of olivine from Kīlauea eruptions (1500-2010 C.E.) show that the primary controls on < Fo_{88} olivine NiO contents are fractional crystallization, magma mixing, and diffusive re-equilibration. Core-rim transects of normally zoned olivine crystals reveal marked differences in Fo and NiO zoning patterns that cannot be related solely to fractional crystallization. These Fo-NiO profiles usually occur in olivine with < Fo_{88} and are common in mixed magmas, although they are not restricted to lavas with obvious petrographic signs of mixing. 3D numerical diffusion models show that diffusive re-equilibration decouples the growth zoning signatures of faster diffusing Fe-Mg (Fo) from the somewhat slower Ni. This diffusive 'decoupling' overprints the chemical relationships of Fe-Mg, Ni, and Mn inherited from crystal growth and influences the calculated fraction of pyroxenite-derived melt (Xpx). Sections of numerical olivine that have been affected by diffusive re-equilibration indicate that larger phenocrysts (800 μm along c-axis) are > 50% more likely to preserve original Xpx compared to smaller phenocrysts (400 μm along c-axis) which rarely (6%) recover original Xpx. Sections that are parallel or sub-parallel to the c-axis and/or pass near the core of the crystal best preserve growth signatures. Thus, diffusive re-equilibration, crystal size, and sectioning effects can strongly influence the characterization of mantle source lithologies for Hawaiian volcanoes.

Keywords: Olivine, nickel, Kīlauea, Hawai'i, magma mixing, diffusion, pyroxenite

INTRODUCTION

Hawaiian olivine from tholeiitic basalts are enriched in Ni compared to those from mid-ocean ridge basalts (MORB) at a given forsterite content (Fig. 1). This enrichment is a feature that has received much attention, with diverse interpretations (source and crustal) regarding its origin

(e.g. Hart and Davis 1978; Sobolev et al. 2005; Wang and Gaetani 2008; Herzberg et al. 2013). One hypothesis advocates that high-Ni parental liquids are produced from olivine-free pyroxenite (i.e. secondary pyroxenite, formed from the reaction of partial melts of eclogite with peridotite; Sobolev et al. 2005; Herzberg 2006; Sobolev et al. 2007). Alternatively, somewhat more siliceous magmas can influence olivine compositions because they cause higher partition coefficients for nickel in olivine (e.g. $D_{Ni}^{ol/melt}$=12.5-22.5 for eclogite melt compared to 7.5-12.5 for basaltic melts; Wang and Gaetani 2008), alleviating the need for a multi-stage process to form an olivine-free pyroxenite hybrid source component. Differences in melting and crystallization temperatures can also strongly influence $D_{Ni}^{ol/melt}$ (Hart and Davis 1978; Kinzler et al. 1990; Matzen et al. 2013) but are unlikely to affect Hawaiian olivine Ni variability because: (1) the age of the oceanic crust under the Hawaiian Islands is 85-95 Myr so decreasing plate age would have a minimal effect on the plate thickness (i.e. melting T) for this relatively old oceanic crust (Parsons and Sclater 1977; Müller et al. 2008), (2) the difference in melting temperature between major Hawaiian volcanoes is small (<60 °C; Putirka et al. 2011), and (3) variations in crystallization temperature between Hawaiian volcanoes probably do not produce resolvable variations in olivine Ni content (Matzen et al. 2013).

Crustal magmatic processes can also have a significant influence on olivine compositions (e.g. Herzberg et al. 2014, 2016). Fractional crystallization has been shown to strongly affect $D_{Ni}^{ol/melt}$ as a result of changing melt composition, producing steep olivine Fo-NiO trends at high Fo that are distinct from shallower trends associated with batch or equilibrium crystallization (Hart and Davis 1978; Beattie et al. 1991; Wang and Gaetani 2008). Magma mixing and diffusive re-equilibration, important processes in Hawaiian magmas, control the composition of erupted magma and element zoning in olivine (e.g. Wright and Fiske 1971; Yang et al. 1999).

Diffusive re-equilibration occurs relatively rapidly at basaltic temperatures (Chakraborty 2010 and references therein) and produces shallow linear trends that broaden the NiO variability at a given Fo (Wang and Gaetani 2008). Determining the contributions of these processes to the overall NiO variability in Hawaiian olivine is essential for distinguishing the influence of crustal and mantle processes on the degree of olivine NiO enrichment.

Hawai‘i is the ideal location to study the relative effects of mantle and crustal processes on the NiO content in olivine because: (1) there are good constraints on the lithosphere and crustal thickness (e.g. Parsons and Sclater 1977; Li et al. 2004), (2) the generation and magmatic evolution of mafic magmas has been extensively examined (e.g. Yoder and Tilley 1962; Green and Ringwood 1967; Wright and Fiske 1971; Eggins 1992; Takahashi and Nakajima 2002) and (3) most Hawaiian tholeiites are mineralogically simple with only olivine as a phenocrystic phase (e.g. Wright 1971; Garcia et al. 1989). Thus, the complications of multi-phase crystallization can generally be avoided (e.g. Shorttle and Maclennan 2011). There is also a wealth of published data on olivine and host lavas for many of the major Hawaiian volcanoes (Fig. 2) allowing comparisons of lava and mineral chemistry (e.g. Garcia et al. 1995; Sobolev et al. 2007; Putirka et al. 2011).

The Ni contents of Hawaiian olivine are examined here from two perspectives: variations between major volcanoes (Fig. 2) and variations observed for individual volcanoes. First, the parental melt and olivine compositions from five Hawaiian shield volcanoes (Ko‘olau, Mauna Loa, Mauna Kea, Kīlauea, and Lō‘ihi) are compared. Calculations of melt polymerization (Mysen et al. 1985) and $D_{Ni}^{ol/melt}$ (e.g. Wang and Gaetani 2008) are used to divide these volcanoes into high- and low-Ni groups that are dominantly controlled by parental melt compositions. Second, variations in melt and olivine compositions within one volcano (Kīlauea) are examined

in samples for which magmatic conditions can be well constrained. Minor variations in parental melt NiO contents (0.09-0.11 wt%) account for the range of NiO contents for ≥ Fo_{88} olivine crystals. Much of the Ni variation for <Fo_{88} olivine in Kīlauea lavas can be explained by shallow magmatic processes (principally storage, crystallization, and mixing), wherein diffusive re-equilibration can have a significant impact on the chemical relationships inherited by growth.

SAMPLES AND METHODS

Modal mineralogy for 14 samples from the long lived, ongoing Pu‘u ‘Ō‘ō eruption (Fig. 2), upper east rift zone (ERZ; not including Pu‘u ‘Ō‘ō), and summit eruptions were determined using 300 counts per sample (excluding vesicles) for phenocrysts (> 0.5 mm), microphenocrysts (0.1-0.5 mm), and matrix (glass and small crystals < 0.1 mm). The Kīlauea lavas and tephra used for this study are glassy and weakly to moderately olivine-phyric, with 1-7 vol. % phenocrysts and/or microphenocrysts (Table 1). Olivine is almost always the only phenocryst in these samples, usually with rare equant spinel inclusions < 0.1 mm in diameter. Pu‘u ‘Ō‘ō lavas erupted between 1990 and 2010 are less olivine-phyric than those erupted earlier. Clinopyroxene and plagioclase phenocrysts are absent or rare (< 1.5 vol. %; Table 1) in Pu‘u ‘Ō‘ō lavas. When present, they occur as microlites (< 0.1 mm) or rarely as microphenocrysts in lavas erupted from 2006-2010. The groundmass of all samples is typically light brown glass or black cryptocrystalline matrix. Most Kīlauea samples were collected in a molten state and quenched with water to minimize post-eruption crystallization. Sample numbers (e.g. 4-Aug-00) refer to the date it was collected in a molten state. Episodes (Ep.) 1-12 from the Pu‘u ‘Ō‘ō eruption were selected for detailed olivine analyses because magma mixing was documented as a dominant process throughout that time period (e.g. Garcia et al. 1992).

High precision olivine analyses were made using a five spectrometer JEOL Hyperprobe JXA-8500F at the University of Hawai‘i. Compositions were determined for 519 olivine crystals (Table 2 and Supplementary Data File 2) from Kīlauea lavas that span a wide compositional range (whole-rock MgO 7.0-10.1 wt%). Olivine spot analyses were done using a 20 kV accelerating voltage and a 200 nA beam current with a diameter of 10 μm. Peak counting times for analyses that included Mn (used for calculating percent pyroxenite in the melt) were 100 s for Si, Mg, Ca and Ni, 60 s for Mn, and 30 s for Fe. A more efficient routine without Mn and with shorter peak counting times (40-60 s for Si, Fe, Ni, Mg and Ca) was used for core-rim traverses. Backgrounds for all analyses were measured on both sides of the peak for half the peak counting times. Traverses in olivine were made using a 2 μm beam diameter and a 5 μm spacing and were oriented perpendicular to well-formed crystal faces away from corner locations to reduce sectioning effects on zoning patterns (Pearce 1984; Shea et al. 2015). Standards were San Carlos olivine (USNM 111312/444; Jarosewich et al. 1980) for Si, Fe and Mg, a synthetic nickel-oxide for Ni, Verma garnet for Mn and Kakanui Augite (USNM 122142; Jarosewich et al. 1980) for Ca. Two sigma relative precision for analyses, based on repeated analysis of San Carlos olivine, are 0.68 wt% for SiO_2, 0.38 wt% for MgO, 0.15 wt% for FeO, 0.008 wt% for NiO, 0.004 wt% for MnO, and 0.006 wt% for CaO (for analyses that included Mn) and 0.78 wt% for SiO_2, 0.44 wt% for MgO, 0.13 wt% for FeO, and 0.02 wt% for NiO and CaO (for analyses that did not include Mn). X-ray intensities were converted to concentrations using standard ZAF corrections (Armstrong 1988). Analyses with totals < 99.0 wt% or > 100.5 wt% were rejected. Each olivine data point represents an average (reported in Table 2 and Supplementary Data File 2) of two to three analyses at the center of the crystal determined by observation of geometry and intensity of zoning in BSE images. Olivine datasets for shield stage tholeiitic basalts from the literature

(Garcia 2002; Sobolev et al. 2007) were filtered for analysis quality (e.g. >99.0 wt% and <100.5 wt%).

RESULTS

Kīlauea olivine cores have a wide range in NiO at a given Fo (e.g. 0.29-0.42 wt% at Fo_{87}; Fig. 3). Olivine from Pu‘u ‘Ō‘ō samples can be divided into two groups: higher Ni for Ep. 1-12 and lower Ni for Ep. 48-58 olivine. Most Pu‘u ‘Ō‘ō Ep. 1-12 olivine crystals have core forsterite compositions that are too high to be in equilibrium with their host-rock Mg-number (Mg# = [Mg/(Mg+Fe^{2+}) x 100]; Fig. 4). Some lavas with an Mg# of 59-60 have olivine compositions that plot both above and below the equilibrium field (e.g. Ep. 1-12; Fig. 4). These lavas have bimodal olivine Fo populations with both normally and reversely zoned crystals, consistent with the inferred history of magma mixing for these episodes (e.g. Garcia et al. 1992). Olivine crystals from Ep. 48-58, a period when the lavas have no obvious petrographic signs of mixing (except Ep. 54, not shown here; Garcia et al. 2000; Thornber et al. 2003) are either in equilibrium with their whole-rock Mg# or are more magnesian than their host whole-rock would suggest at equilibrium (dashed black lines; Fig. 4). These olivine crystals are normally zoned and may reflect delayed fractionation (Maaløe et al. 1988) indicating a simpler magmatic history compared to Ep. 1-12 samples.

Core-rim transects of Kīlauea olivine crystals reveal two distinct Fo and NiO zoning patterns. Typically, olivine in equilibrium with their whole-rock Mg# have simple normal zoning profiles (e.g. Pearce 1984), where Fo and NiO co-vary and have similar concentration plateaus followed by similar decreases toward the rim (‘coupled’ profile, Fig. 5). Some Kīlauea olivine crystals have distinctly different Fo and NiO zoning morphologies with a wider NiO plateau in

their core compared to Fo ('decoupled' profile, Fig. 5), similar to those observed by Nakamura (1995). Decoupled crystals are found throughout the Pu'u 'Ō'ō eruption and always have Fo compositions above the equilibrium field with respect to their whole-rock Mg# (Fig. 4), suggesting that decoupling is a feature of olivine crystals that are from mixed magmas.

DISCUSSION

The origin of Ni-rich olivine in Hawaiian lavas is controversial. An olivine-free pyroxenite and/or eclogite source has been invoked to explain the high Ni contents (e.g. Sobolev et al. 2007; Wang and Gaetani 2008). Previous studies focused primarily on mantle processes for generating the Ni-enriched, Makapu'u (Ko'olau) olivine (e.g. 0.60 wt% NiO at >Fo_{88}; Fig. 1). The goal here is to examine other potential causes for the observed NiO differences in olivine between five Hawaiian volcanoes (inter-volcano variability) and at individual volcanoes (intra-volcano variability) in order to evaluate the relative contributions of mantle and crustal processes. First, inter-volcano variability is explored through investigations of parental melt composition, $D_{Ni}^{ol/melt}$, and the NiO contents of primitive olivine. Intra-volcano variations are examined using high precision analyses of olivine to assess the influence of crustal processes such as crystallization, magma mixing, and diffusive re-equilibration on interpretations of mantle source lithology.

Inter-volcano Ni variability

The wide range of Hawaiian olivine composition can be subdivided into two groups based on the average NiO at a given Fo (Fig. 1, regression lines). Olivine in lavas from Ko'olau, Mauna Kea, and Mauna Loa form a broad, crescent shaped Fo-NiO field (upper insert; Fig 1) with a 0.25-

185 0.60 wt% range in Ni at Fo_{88} (high-Ni group). Olivine from Kīlauea and Lō‘ihi lavas form flatter
186 Fo-NiO trends (lower insert, Fig. 1) with a narrower range in NiO (0.27-0.43 wt% at Fo_{88}; low-
187 Ni group). The division of the high- and low-Ni volcano groups is likely unrelated to parental
188 liquid Ni content, as there is no systematic difference in whole-rock Ni between lavas from
189 different Hawaiian volcanoes for a large range of MgO (Fig. 6a). Evolved lavas (<7.0 wt%
190 MgO) were not considered in this study to avoid the complicating effects of multi-phase
191 fractionation (e.g. Shorttle and Maclennan 2011). Lavas with MgO >10.5 wt% are likely affected
192 by olivine accumulation (e.g. Hart and Davis 1978; Garcia 1996; Rhodes et al. 2012), although
193 are similar to parental melt compositions (e.g. Putirka et al. 2011).
194 Ko‘olau, Mauna Loa, and Mauna Kea lavas have whole-rock Ni that lie on both sides of
195 the Hart and Davis (1978) line and overlap considerably with 20th and 21st century Kīlauea
196 samples (Fig. 6a). However, olivine from these volcanoes display significant differences in
197 maximum NiO contents (e.g. up to 0.22 wt%) at Fo_{88} (Fig. 1). This issue was highlighted by
198 Rhodes et al. (2012), who showed that there is no relationship between the olivine NiO contents
199 and the SiO_2 contents of lavas from Mauna Loa and Mauna Kea (even for lavas with 30 wt%
200 MgO), contrary to what would be expected if the source for the parental melts were an olivine-
201 free pyroxenite hybrid. Furthermore, there is considerable Ni variation at a given MgO content
202 for peridotites (e.g. 1200-3200 ppm Ni at 40% MgO; Rhodes et al. 2012), and when coupled
203 with current uncertainties in estimating the partitioning of Ni between olivine and melt, melting
204 of peridotite could account for Ni and SiO_2 variability observed in Hawaiian basalts (Putirka et
205 al. 2011; Rhodes et al. 2012).
206

Influence of parental melt composition on $D_{Ni}^{ol/melt}$. Lavas from the low-Ni group volcanoes (Kīlauea and Lōʻihi) have 1-5 wt% lower SiO_2 than those from the high-Ni group at the same MgO contents (Koʻolau, Mauna Loa, and Mauna Kea; e.g. Garcia et al. 1989; Rhodes et al. 1989; Frey et al. 1994). Variations in SiO_2 in Hawaiian basalts have been explained by variable degrees of melting of eclogite and/or peridotite (e.g. Takahashi and Nakajima 2002; Putirka et al. 2011; Rhodes et al. 2012). Experimental studies have also shown that Ni partitioning increases significantly with increasing melt polymerization (higher SiO_2), yielding high NiO olivine in more siliceous melts (e.g. Hart and Davis 1978; Wang and Gaetani 2008). The increase in $D_{Ni}^{ol/melt}$ with increasing SiO_2 is hyperbolic (Wang and Gaetani 2008). Thus, the small observed differences in parental melt SiO_2 (1-5 wt%) may potentially affect $D_{Ni}^{ol/melt}$ significantly. The magnitude of this effect is evaluated below.

Parental melt compositions (Table 3) for each volcano were calculated by incremental addition of olivine in equilibrium with the melt until added olivine reached Fo_{91} (the maximum Fo measured in Hawaiian lavas; Garcia et al. 1995), an approach that was used by Putirka et al. (2011) to estimate Hawaiian parental magma compositions. Parental melt NiO values of 0.09 wt% and 0.11 wt% NiO (i.e. 707-864 ppm Ni, expressed as elemental concentration) were used, similar to the parental Ni contents suggested by Sobolev et al. (2005) and Putirka et al. (2011). A pressure of 1 GPa and a starting temperature of 1450 °C were determined with MELTS (Ghiorso and Sack 1995; Asimow and Ghiorso 1998) and used in the model runs. The ratio of non-bridging oxygen to tetrahedrally-coordinated cations (NBO/T; Mysen et al. 1985) was calculated to approximate the degree of polymerization for each parental melt composition along its fractional crystallization trend. These ratios were used to calculate the Ni partition coefficient of

229 Wang and Gaetani (2008), which is sensitive to variations in SiO_2, a major component of
230 NBO/T.

231 The Ko‘olau parental magma had the lowest calculated NBO/T for Fo_{91} olivine (1.36),
232 the Mauna Loa and high-SiO_2 Mauna Kea parental magmas are intermediate (1.45), and Kīlauea
233 and low-SiO_2 Mauna Kea (1.61) and Lō‘ihi (1.66; Fig. 7a) are the highest. These NBO/T values
234 equate to $D_{Ni}^{ol/melt}$ values (using the equation of Wang and Gaetani 2008) of 4.3 (Ko‘olau), 4.25
235 (Mauna Loa and high-SiO_2 Mauna Kea), 4.0 (low-SiO_2 Mauna Kea, Kīlauea) and 3.8 (Lō‘ihi;
236 Fig. 7b) for the crystallization of primitive olivine (e.g. Fo_{90}). Olivine compositions were
237 calculated along a liquid line of descent from each volcano’s parental magma using both the
238 $D_{Ni}^{ol/melt}$ and $Kd_{Fe\text{-}Mg}^{ol/melt}$ of Wang and Gaetani (2008; Fig. 8a). The resulting olivine crystallization
239 paths were also compared to crystallization models that used the $D_{Ni}^{ol/melt}$ from Matzen et al. (2013)
240 with $D_{Mg}^{ol/melt}$ calculated from Putirka (2008) and a constant $Kd_{Fe\text{-}Mg}^{ol/melt}$ of 0.32 (Fig. 8b). Previous
241 partitioning approaches (e.g. Hart and Davis 1978; Kinzler et al. 1990; Beattie et al. 1991; Toplis
242 2005; Li and Ripley 2010; Putirka et al. 2011) have been thoroughly compared and discussed in
243 both Wang and Gaetani (2008) and Matzen et al. (2013). Incorporation of the melt composition
244 dependent $Kd_{Fe\text{-}Mg}^{ol/melt}$ expression of Toplis (2005) showed no difference in olivine compositions >
245 Fo_{88} (see Supplementary Material).

246 Both models reproduce the relative NiO enrichment of primitive olivine compositions
247 between volcanoes, with Ko‘olau olivine having the highest NiO and Lō‘ihi olivine the lowest.
248 The Wang and Gaetani (2008) model reproduces the steep Fo-NiO trends for >Fo_{88} olivine
249 compositions better than Matzen et al. (2013), although the NiO contents of Fo_{90} olivine are
250 better matched by the Matzen et al. (2013) approach. Regardless of the partitioning models used,
251 the relative inter-volcano differences are reproduced independent of variations in parental melt

Ni content (Fig. 8). This is consistent with the interpretations of Rhodes et al. (2012) who also compared the partitioning models of Beattie et al. (1991) and Putirka et al. (2011). Models from parental magmas with 0.11 wt% NiO provide a good match the highest compositions observed for each volcano, whereas parental magmas with 0.09 wt% NiO reproduce the lower Ni trends (Fig. 8). Thus, minor variations in parental melt Ni contents account for the range of NiO contents for $\geq Fo_{88}$ olivine.

Intra-volcano Ni variability

Variations in olivine composition within Kīlauea volcano and its long lived (33-year) Pu‘u ‘Ō‘ō eruption provide additional insight into the mantle and crustal processes that control Ni concentrations in Hawaiian basalts. There is substantial variation in whole-rock Ni among weakly olivine phyric Kīlauea basalts at a given MgO concentration (e.g., 75 ppm variability at 9.5 wt% MgO; Fig. 6b). A wide range is also observed for lavas from a single eruption (e.g. Pu‘u ‘Ō‘ō, 60 ppm or 20% relative to median at 9.0 wt% MgO; Fig. 6b). Lavas erupted at the summit and east rift zone (including Ep. 1-30 of the Pu‘u ‘Ō‘ō eruption) almost always lie above the Hart and Davis (1978) line with higher whole-rock Ni compared to lavas erupted from 1988-2010 (Pu‘u ‘Ō‘ō Ep. 31-60; Fig. 6b). Despite the differences in whole-rock Ni, olivine from Ep. 48-58 lavas overlap with summit and east rift zone compositions (Fig. 3). Olivine compositions from Ep. 1-12 are somewhat elevated in Ni at $< Fo_{85}$ but also overlap with summit and east rift zone analyses (Fig. 3). These observations show that melt Ni contents do not correlate with olivine compositions, suggesting that other processes are affecting the NiO content of $< Fo_{88}$ olivine in Kīlauea magmas. Below, the effects of fractional crystallization, magma mixing, and diffusive re-equilibration on olivine Ni contents in Kīlauea lavas are examined.

Crystallization. The olivine Fo-NiO trends for Kīlauea lavas (Fig. 3) can be partly explained by fractional crystallization (Hart and Davis 1978; Wang and Gaetani 2008), which rapidly depletes Ni from the melt and produces steep, positive Fo-NiO trends for early crystallizing olivine from parental liquids (e.g. Kīlauea summit and ERZ olivine; Fig. 3). These observations are consistent with many studies that have identified olivine fractionation as a dominant crustal process at Kīlauea and other Hawaiian volcanoes (e.g. Powers 1955; Wright 1971; Garcia 2002). Delayed fractionation, where magmas undergo extensive cooling and crystallization before fractionation takes place (Maaløe et al. 1988), may account for the range of Fo contents exhibited by many Kīlauea lavas and the presence of olivine with more primitive compositions than predicted (Fig. 4).

The high- and low-Ni volcano groups can also be reproduced via fractional crystallization models from parental magmas with the same NiO contents (Fig. 8). The changing $D_{Ni}^{ol/melt}$ during fractional crystallization (as a function of changing melt composition) creates Fo-NiO trends that are shallower than those observed for < Fo_{88} olivine at all volcanoes, suggesting that other processes control the compositions of these more evolved olivine. Mauna Kea compositions span the two Ni groups with the high-Si parental melt producing olivine similar to the highest NiO observed, and the low-Si parental melt forming lower NiO olivine (Fig. 8). This accounts for some of the wide range of olivine NiO contents observed for Mauna Kea at Fo_{90}. As discussed above, slight variations in the parental melt Ni contents (e.g. 0.09-0.11 wt% NiO) can additionally explain the observed range of olivine NiO contents at ≥ Fo_{88} for each volcano (Fig. 8).

298 **Magma mixing.** The high-NiO olivine from the mixed Ep.1-12 of the Pu‘u ‘Ō‘ō eruption define
299 a somewhat shallower Fo-NiO trend compared to Ep. 48-58 (Fig. 3). If the compositions of these
300 olivine were controlled by the higher whole-rock Ni of their host lavas and subsequent fractional
301 crystallization, the trend should be parallel to and elevated above the later Ep. 48-58 olivine. This
302 divergence in observed Fo-NiO trends requires that some other process is involved. Many of the
303 Ep. 1-12 olivine are out of equilibrium with their whole-rock Mg#, have decoupled Fo-NiO
304 profiles, and are from lavas that contain both normally and reversely zoned olivine crystals (Fig.
305 4 and 5). These features are indicative of magma mixing, which agrees with previous
306 interpretations based on whole-rock geochemistry (e.g. Garcia et al. 1989, 1992). The Ep. 1-12
307 mixing trend is generated as olivine crystallizes from and diffusively re-equilibrates with the
308 mixed magmas (Wang and Gaetani 2008). Olivine crystals that have undergone protracted
309 diffusive re-equilibration have higher Ni at a given Fo compared to olivine compositions
310 produced by fractional crystallization (e.g. Ep. 1-12 vs. 48-58 of Pu‘u ‘Ō‘ō; Fig. 3). The effect of
311 this relative Ni enrichment is more pronounced for evolved compositions (e.g. $Fo_{80\text{-}85}$, Fig. 3).
312 The fractional crystallization models (Fig. 8) generated $<Fo_{85}$ olivine with lower Ni than
313 is observed in the natural dataset. The natural olivine compositions are probably affected by
314 magma mixing (Fig. 3) and/or other processes, which causes the Fo-NiO trend to become
315 shallower than the fractional crystallization only trends produced by the models (Fig. 8). Mixing
316 of relatively more primitive and more evolved melts produced by fractional crystallization with
317 variable $D_{Ni}^{ol/melt}$ contributes to a broad crescent-shaped Fo-NiO field for Ko‘olau, Mauna Loa, and
318 Mauna Kea (upper insert; Fig. 1) due to the relatively high NiO in primitive olivine equilibrating
319 with more evolved compositions. A lower NiO content for $\geq Fo_{88}$ olivine at Kīlauea and Lō‘ihi

leads to a narrower range of compositions that mix and produce the more limited Ni array (lower insert, Fig. 1).

Diffusive re-equilibration. The extent of diffusive re-equilibration of individual chemical species is largely dependent on (1) the relative diffusivities of the cations (e.g. $D_{Fe\text{-}Mg} \approx D_{Mn} > D_{Ni} > D_{Ca}$; Chakraborty 2010 and references therein) and (2) the contrast in element concentration between the olivine and the surrounding melt. To quantify the development of elemental decoupling by diffusion, numerical models were used to simulate diffusive re-equilibration of Fo and Ni in olivine. A concentration dependent, 3D diffusion equation (three spatial dimensions *x*, *y*, and *z* in addition to time *t*) was implemented following the methods described in Shea et al. (2015) to allow Fe-Mg and Ni to diffuse simultaneously. The olivine+melt model had dimensions of 221 x 221 x 221 voxels with each voxel being 4 x 4 x 4 μm. The olivine has a dimension of 201 voxels along the c-axis, 123 voxels along the b-axis, and 94 voxels along the a-axis (Fig. 9). The resulting olivine is ~800 x 500 x 375 μm, comparable to the size of larger olivine in Kīlauea lavas (e.g. Vinet and Higgins 2011). The volume of melt around the crystal, although limited in the model, was an infinite reservoir for diffusing species and as such an infinite boundary condition. Magmatic conditions appropriate for Kīlauea were used, including a pressure of 85 MPa (within the depth range for Kīlauea's summit reservoir, 2-5 km; Cervelli and Miklius 2003; Poland et al. 2014) assuming a crustal density of 2.9 kg/km^3. The oxygen fugacity was set at ΔQFM -1 (Rhodes and Vollinger 2005) and temperature was held constant at 1200 °C, which is appropriate for a Kīlauea magma with 9.25 wt% MgO based on the experimental work of Helz and Thornber (1987). Model runs simulated diffusive re-equilibration for 1 and 2 years, which are within the 0.5-8 years magma residence time estimate for historical

Kīlauea lavas (Pietruszka et al. 2015). Diffusivities for Fe-Mg and Ni were taken from Dohmen and Chakraborty (2007) and Chakraborty (2010) respectively. Olivine models were sectioned perpendicular to the c-axis through the core of the crystal, and core-rim profiles were sampled along the b-axis (Fig. 9).

Variations in the extent of diffusion between chemical species are described by % re-equilibration (req), which is used to normalize the absolute concentration change of each element and allow their direct comparison (Eq. 1),

$$\%\, req = \frac{(C_{initial} - C_{measured})}{(C_{initial} - C_{equilibrium})} * 100 \quad (1)$$

where $C_{initial}$ is the composition of olivine inherited from crystal growth before the onset of diffusion, $C_{measured}$ is the measured composition of the olivine after diffusion, and $C_{equilibrium}$ is the composition of the surrounding melt (expressed as the Fo content of an olivine in Fe-Mg equilibrium with the melt; Fig. 10a). NiO and Fo contents were chosen based on natural compositions from the high-Fo end of the Hawaiian olivine dataset (Fig. 1). The numerical olivine had $C_{initial}$ of Fo_{90} and 0.60 wt% NiO and $C_{equilibrium}$ of Fo_{85} and 0.35 wt% NiO (Fig. 9).

The model results show that the decoupled Fo-NiO profiles associated with magma mixing at Kīlauea are produced by diffusion (Fig. 10a). The decoupling is caused by the slower diffusion of Ni compared to Fe-Mg, as shown by Dohmen and Chakraborty (2007) and Petry et al. (2004). The faster diffusion of Fe-Mg in olivine produces shorter core plateau lengths for Fo than NiO in the same crystal (e.g. Fig. 5 and 10a). Although Ni diffusivity can vary with melt SiO_2 (Zhukova et al. 2014), this effect is negligible for Hawaiian lavas given their small observed ranges in melt SiO_2 (1-5 wt%; see Supplementary Data File 3 for diffusivity calculations). High-

366 Fo olivine mixed with fractionated basaltic melt produces olivine with normal zoning, in which
367 olivine crystals re-equilibrate to more Fe rich, Mg poor (e.g. lower Fo) and Ni poor compositions
368 (Fig. 5 and 10a). With time, olivine crystals develop lower Fo at a faster rate than the decrease of
369 Ni, resulting in compositions that would not be expected from fractional crystallization alone
370 (e.g. Nakamura 1995). The penetration distance and degree of diffusive re-equilibration in the
371 olivine increases with time (Fig. 10b). Thus, olivine compositions that have been affected by
372 diffusive re-equilibration probably do not preserve chemical relationships inherited from crystal
373 growth.
374
375 **Characterizing source lithology using olivine composition.**
376 Olivine major and minor elements have been used to calculate the weight fraction of
377 pyroxenite derived melt in the source (Xpx; Sobolev et al. 2005, 2007; Gurenko et al. 2010). A
378 potential flaw in this method is the use of element ratios (e.g. Li and Ripley 2010) which can be
379 affected by crustal processes. To more fully characterize the extent to which crustal processes
380 affect estimates of source lithology, we examined the influence of diffusive re-equilibration on
381 the calculated pyroxenite content in both natural olivine and numerical model olivine crystals.
382 Decoupling of Fo and NiO in olivine (Fig. 10b) may modify the recorded fraction of
383 pyroxenite derived melt (Xpx) because concentration of Ni, Mn, FeO, and MgO are used to
384 make these calculations (e.g. Sobolev et al. 2005) as in this example (Gurenko et al. 2010; Eq.
385 2):
386
387 $$X_{px} = 6.70E-04 \times Ni \times \frac{FeO}{MgO} - 1.332E-02 \times \frac{Mn}{FeO} + 1.524 \quad (2)$$
388

As a high-Fo olivine becomes normally zoned, FeO increases as MgO decreases, resulting in an increase in the FeO/MgO ratio (Eq. 2). This increase has a larger impact on calculated pyroxenite than the decrease of Ni during diffusion due to (1) the slower diffusivity of Ni and (2) the amplifying effect of increasing FeO while simultaneously decreasing MgO. Olivine from Kīlauea can be strongly zoned in Fo (e.g. 78-86.5 %; Fig. 11a) with complex growth and diffusion histories. From the core of the example olivine to its rim, diffusive re-equilibration of Fe-Mg, Ni, and Mn increased the calculated pyroxenite fraction from ~50% to 100% (Fig. 11b) and then decreased again to ~67%. This natural example suggests that diffusive re-equilibration can significantly raise and/or lower the measured pyroxenite component (by at least 50%), creating significant spread in the inferred lithology of the mantle source region.

To determine whether diffusive re-equilibration strongly affects olivine core compositions, we compared numerical olivine models of different sizes (along their c-axis): 800 μm ("large", consistent with antecryst sizes in Kīlauea lavas; e.g. Vinet and Higgens 2011) and 400 μm ("small", a size that is common in many Kīlauea lavas, especially those from Pu'u 'Ō'ō; Table 1). Models simulated two years of diffusion at 1200 °C for Fe-Mg (Fo), NiO, and MnO. Crystal ($C_{initial}$) and melt ($C_{equilibrium}$) compositions of $Fo_{initial}$=90, $NiO_{initial}$=0.60 wt%, $MnO_{initial}$=0.13 wt% , $Fo_{equilibrium}$=82, $NiO_{equilibrium}$=0.25 wt%, and $MnO_{equilibrium}$=0.23 wt% were used. Numerical olivine crystals from both models were randomly sliced 250 times, the Ni and Mn (ppm) and FeO and MgO (wt%) core compositions in each crystal section were "measured" (see Supplementary Material and Data File 4), and the results were used to calculate the weight fraction of pyroxenite-derived melt using Eq. 2 (Gurekno et al. 2010).

The model sections of the large olivine had an average composition of $Fo_{88.8}$ compared to the original Fo_{90}. About 60% of the sections returned original Xpx within ±1% of the original

412 value (e.g. 76-78% Xpx). The section types most likely to retain original compositions were
413 oriented parallel or sub-parallel to the c-axis and/or near to the core of the crystal (Fig. 12). In
414 contrast, the small model thin section had an average of Fo_{86} and only 6% recovered the original
415 Xpx within ±1%. The small olivine had sections with core compositions that were on average
416 more re-equilibrated (e.g. 50% re-equilibration) compared the large crystal (13% re-
417 equilibration). In both models, the calculated Xpx ranged up to 87-89%, more than 10% higher
418 than the 77% Xpx from the original composition. The small crystal also had a considerable range
419 of Xpx below the original value (minimum was 67%), indicating that these highly re-equilibrated
420 sections reflect the Xpx of the more evolved surrounding melt, not the initial crystal
421 composition. Strikingly, sections from the small crystal taken near to the core and parallel or
422 sub-parallel to the c-axis rarely recovered initial Xpx These example models indicate that at least
423 a 20% range in Xpx is recoverable if the olivine have been affected by diffusive re-equilibration,
424 and the natural example (Fig. 11b) suggests even greater variability is possible if the
425 compositional difference between the phenocryst and surround melt is more significant.
426 Regardless of crystal size, sectioning a natural olivine phenocryst parallel or sub-parallel
427 to the c-axis is statistically rare due to its relatively elongate geometry (Fig. 9). Crystals are more
428 likely to be sectioned in some manner sub-perpendicular to the c-axis (Fig. 12, see also
429 Supplementary Fig. S2). Larger crystals should generally be more reliable for using olivine
430 compositions to infer characteristics about source componentry. The core compositions of these
431 larger crystals are, however, decoupled and compromised after ~6 years of diffusive re-
432 equilibration based on model conditions described above. These storage timescales are not
433 unreasonable, considering recent estimates of magma storage within Kilauea range from 0.5-8

434 years (Pietruszka et al. 2015). Thus, some knowledge of the storage histories of olivine cargo is
435 required if using their compositions to investigate mantle processes.
436

437 ## IMPLICATIONS

438 This study highlights the complexities associated with the modifying effects of crustal
439 processes and inferring characteristics about mantle source lithologies. In light of the numerous
440 hypotheses regarding the origin of Hawaiian basalts, our study clearly illustrates that crustal
441 processes are a significant factor in contributing to these diverse interpretations. Even parental
442 melt characteristics (e.g. SiO_2), which are inherited during melt generation, can strongly control
443 $D_{Ni}^{ol/melt}$ and the compositions of primitive olivine. New modeling investigations presented here
444 provide evidence that subsequent diffusive re-equilibration of Fe-Mg, Mn, and Ni in olivine can
445 rapidly overprint the chemical relationships inherited during growth, thereby strongly affecting
446 the calculated pyroxenite component and inducing 20-50% (or more) variability. The numerical
447 olivine may provide minimum constraints, as the mixing end member compositions could vary
448 substantially and greater differences in melt Mg# would induce greater extents of diffusive re-
449 equilibration and elemental decoupling.

450 The effects of diffusion on olivine composition are further complicated by random
451 sectioning of crystals. In natural samples, ideal sections are rare (e.g. Pearce 1984; Fig. 12). The
452 vast majority of olivine in a typical thin section are cut off center and oblique to principle axes
453 (Shea et al. 2015). Diffusive re-equilibration will substantially modify the FeO/MgO, Ni, and
454 Mn/FeO in these sections due to the different diffusivities of these elements. Thus, olivine
455 crystals of moderate size that grow and are stored in the crust for a few years are unlikely to
456 preserve their original crystallization history. These effects are significant for smaller crystals

457 (e.g. < 0.5 mm along c-axis), which should be avoided in estimating the composition of the
458 source components. Large, high Fo (≥ 88) olivine crystals are likely less affected by a few years
459 of diffusive re-equilibration if sectioned near or through the crystal core and are more
460 appropriate for analyses that will be used to characterize mantle processes if there are good
461 constraints on magma storage and transport histories. Furthermore, large crystals like those
462 found in picrites are more likely to retain growth compositions after a few years of diffusive re-
463 equilibration and are potentially more reliable indicators of source lithology in Hawaiian lavas
464 (although some sense of their storage histories are required). Our results raise concerns regarding
465 the use of olivine major and minor elements to characterize source lithologies for Hawaiian
466 volcanoes and suggest that their olivine compositions can be unreliable records of mantle source.
467 This work emphasizes how rapidly olivine compositions are compromised in relatively high
468 temperature basaltic systems, particularly when the inherent complexities of natural samples are
469 considered. Due to numerous variables (e.g. diffusion duration, crystal size, heterogeneous vs.
470 homogeneous populations) these numerical examples represent a simple case scenario, and
471 suggest that diffusion could have a significant influence on interpretations drawn from olivine
472 major and minor element compositions.
473

474 **ACKNOWLEDGEMENTS**

475 The authors acknowledge Keith Putirka, Benoît Welsh, and Dawn Sweeny-Ruth for fruitful
476 discussions on olivine growth and compositional zoning, Mike Vollinger for XRF analyses, Eric
477 Hellebrand for assistance with EPMA analyses, Jared Marske for unpublished east rift zone XRF
478 data, and Garrett Ito for access to the Department of Geology and Geophysics, Geophysics and
479 Tectonics Division's computer cluster for diffusion modeling. We thank Claude Herzberg and

480 Andrew Matzen for their helpful formal reviews, and Bruce Watson for editorial handling. The
481 comments from the GG616 Scientific Writing class are also appreciated. This work is supported
482 by NSF Grants EAR11-18741 and EAR13-347915 to MG, EAR13-21890 to TS, the Fred M.
483 Bullard Foundation and the University of Hawai‘i Graduate Student Organization to KL. This is
484 SOEST contribution number XXXX.
485

References Cited

Armstrong, J. T. (1988) Quantitative analyses of silicate and oxide materials: Comparison of Monte Carlo, ZAF, and φ(ρz) procedures. In Microbeam Analyses, D.E. Newbury, Ed., San Francisco Press, San Francisco, pp 239-246.

Asimow, F.D., and Ghiorso, M.S. (1998) Algorithmic modifications extending MELTS to calculate subsolidus phase relations. American Mineralogist, 83, 1127-1131.

Beattie, P., Ford, C., and Russel, D. (1991) Partition coefficients for olivine-melt and orthopyroxene-melt systems. Contributions to Mineralogy and Petrology, 109, 212-224.

Byers, C.D., Garcia, M.O., and Muenow, D.W. (1985) Volatiles in pillow rim glasses from Loihi and Kilauea volcanoes, Hawaii. Geochimica et Cosmochimica Acta, 49, 1887-1896.

Cervelli, P.F., and Miklius, A. (2003) The shallow magmatic system of Kilauea Volcano. U.S. Geological Survey Professional Paper, 1676, 149-163.

Chakraborty, S. (2010) Diffusion coefficients in olivine, wadsleyite and ringwoodite. In Diffusion in Minerals and Melts, Zhang, Y., and Cherniak, D.J., Eds., Reviews in Mineralogy and Gochemistry, 72, pp 603-639.

Dohmen, R., and Chakraborty, S. (2007) Fe-Mg diffusion in olivine II: point defect chemistry, change of diffusion mechanisms and a model for calculation of diffusion coefficients in natural olivine. Physics and Chemistry of Minerals, 34, 409-430.

Eggins, S.M. (1992) Petrogenesis of Hawaiian tholeiites: 1, phase equilibria constants. Contributions to Mineralogy and Petrology, 110, 387-397.

Frey, F.A., Garcia, M.O., and Roden, M.F. (1994) Geochemical characteristics of Koolau volcano: Implications of intershield geochemical differences among Hawaiian volcanoes. Geochimica et Cosmochimica Acta, 58, 1441-1462.

509 Garcia, M.O., Ho, R.A., Rhodes, J.M., and Wolfe, E.W. (1989) Petrologic constraints on rift-
510 zone processes. Bulletin of Volcanology, 52, 81-96.
511 Garcia, M.O., Rhodes, J.M., Wolfe, E.W., Ulrich, G.E., and Ho, R.A. (1992). Petrology of lavas
512 from episodes 2-47 of the Puu Oo eruption of Kilauea Volcano, Hawaii: Evaluation of
513 magmatic processes. Bulletin of Volcanology, 55, 1-16.
514 Garcia, M.O., Jorgenson, B.A., and Mahoney, J.J. (1993) An evaluation of temporal geochemical
515 evolution of Loihi summit lavas: Results from Alvin submersible dives. Journal of Geophysical
516 Research, 98, 537-550.
517 Garcia, M.O., Hulseboch, T.P., and Rhodes, J.M. (1995) Olivine-rich submarine basalts from the
518 southwest rift zone of Mauna Loa Volcano: Implications for magmatic processes and
519 geochemical evolution. In Geophysical Monograph 92. Rhodes, J.M. and Lockwood, J.P.,
520 Eds., Mauna Loa Revealed: Structure, Composition, History, and Hazards, p. 219-239,
521 American Geophysical Union, Washington, D.C., USA.
522 Garcia, M.O. (1996) Petrography and olivine and glass chemistry of lavas from the Hawaii
523 Scientific Drilling Project. Journal of Geophysical Research, 101, 11701-11713.
524 Garcia, M.O., Pietruszka, A.J., Rhodes, J.M., and Swanson, K.J. (2000) Magmatic processes
525 during the prolonged Pu´u ´O´o eruption of Kilauea Volcano, Hawaii. Journal of Petrology, 41,
526 967-990.
527 Garcia, M.O. (2002) Submarine picritic basalts from Ko‘olau volcano, Hawaii: Implications for
528 parental magma compositions and mantle source. In Geophysical Monograph 128. Takahashi,
529 Lipman, Garcia, Naka, and Aramaki, Eds., Hawaiian Volcanoes: Deep Underwater
530 Perspectives, 391-401. American Geophysical Union, Washington, D.C., USA.

Garcia, M.O., Pietruszka, A.J., and Rhodes, J.M. (2003) A petrologic perspective of Kīlauea volcano's summit magma reservoir. Journal of Petrology, 44, 2313-2339.

Ghiorso, M.S., and Sack, R.O. (1995) Chemical mass transfer in magmatic processes IV. A revised and internally consistent thermodynamic model for the interpretation and extrapolation of liquid-solid equilibria in magmatic systems at elevated temperatures and pressures. Contributions to Mineralogy and Petrology, 119, 197-212.

Green, D.H., and Ringwood, A.E., (1967) The genesis of basaltic magmas. Contributions to Mineralogy and Petrology, 15, 103-190.

Greene, A.R., Garcia, M.O., Pietruszka, A.J., Weis, D., Marske, J.P., Vollinger, M.J., and Eiler, J. (2013) Temporal geochemical variations in lavas from Kīlauea's Pu'u 'Ō'ō eruption (1983-2010): Cyclic variations from melting of source heterogeneities. Geochemistry, Geophysics, Geosystems, 14, 4849-4873.

Gurenko, A.J., Hoernle, K.A., Sobolev, A.V., Hauff, F., and Schmincke, H.-U. (2010) Source components of the Gran Canaria (Canary Islands) shield stage magmas: evidence from olivine composition and Sr-Nd-Pb isotopes. Contributions to Mineralogy and Petrology, 159, 689-702.

Haskins, E.H., and Garcia, M.O. (2004) Scientific drilling reveals geochemical heterogeneity within the Ko'olau shield, Hawai'i. Contributions to Mineralogy and Petrology, 147, 162-188.

Hart, S.R., and Davis, K.E. (1978) Nickel partitioning between olivine and silicate melt. Earth and Planetary Science Letters, 40, 203-219.

Helz, R.T., and Thornber, C.R. (1987) Geothermometry of Kilauea Iki lava lake, Hawaii. Bulletin of Volcanology, 49, 651-668.

Herzberg, C. (2006) Petrology and thermal structure of the Hawaiian plume from Mauna Kea volcano. Nature, 444, 605-609.

554 Herzberg, C., Asimow, P.D., Ionov, D.A., Vidito, C., Jackson, M.G., and Geist, D. (2013) Nickel
555 and helium evidence for melt above the core-mantle boundary. Nature, 493, 393-397.
556 Herzberg, C., Cabral, R.A., Jackson, M.G., Vidito, C., Day, J.M.D., and Hauri, E.H. (2014)
557 Phantom Archean crust in Mangaia hotspot lavas and the meaning of heterogeneous mantle.
558 Earth and Planetary Science Letters, 396, 97-106.
559 Herzberg, C., Vidito, C., and Starkey, N.A. (2016) Nickel-Cobalt contents of olivine record
560 origins of mantle peridotite and related rocks. American Mineralogist, in press.
561 Jackson, M.C., Frey, F.A., Garcia, M.O., and Wilmoth, R.A. (1999) Geology and geochemistry
562 of basaltic lava flows and dikes from the Trans-Koolau tunnel, Oahu, Hawaii. Bulletin of
563 Volcanology, 60, 381-401.
564 Jarosewich, E., Nelen, J.A., and Norberg, J.A. (1980) Reference samples for electron microprobe
565 analysis. Geostandards Newsletters, 4, 42-47.
566 Kinzler, R.J., Grove, T.L., and Recca, S.J. (1990) An experimental study on the effect of
567 temperature and melt composition on the partition of nickel between olivine and silicate melt.
568 Geochimica et Cosmochimica Acta, 54, 1255-1265.
569 Li, C., and Ripley, E.M. (2010) The relative effects of composition and temperature on olivine-
570 liquid Ni partitioning: Statistical deconvolution and implications for petrological modeling.
571 Chemical Geology, 275, 99-104.
572 Li, X., Kind, R., Yuan, X., Wölbern, I., and Hanka, W. (2004) Rejuvenation of the lithosphere by
573 the Hawaiian plume. Nature, 427, 827-829.
574 Maaløe, S., Pederson, R.B., and James, D. (1988) Delayed fractionation of basaltic lavas.
575 Contributions to Mineralogy and Petrology, 98, 401-407.

576 Marske, J.P., Pietruszka, A.J., Weis, D., Garcia, M.O., and Rhodes, J.M. (2007) Rapid passage of
577 a small-scale mantle heterogeneity through the melting regions of Kilauea and Mauna Loa
578 volcanoes. Earth and Planetary Science Letters, 259, 34-50.
579 Matzen, A.K., Baker, M.B., Beckett, J.R., and Stolper, E.M. (2011) Fe-Mg partitioning between
580 olivine and high-magnesian melts and the nature of Hawaiian parental liquids. Journal of
581 Petrology, 52, 1243-1263.
582 Matzen, A.K., Baker, M.B., Beckett, J.R., and Stolper, E.M. (2013) The temperature and
583 pressure dependence of Nickel partitioning between olivine and silicate melt. Journal of
584 Petrology, 54, 2521-2545.
585 Moore, J.G., and Ault, W.U. (1965) Historic littoral cones in Hawai‘i. Pacific Science, 19, 3-11.
586 Müller, R.D., Sdrolias, M., Gaina, C., and Roest, W.R. (2008) Age, spreading rates, and
587 spreading asymmetry of the world’s ocean crust. Geochemistry Geophysics Geosystems, 9,
588 DOI: 10.1029/2007GC001743.
589 Mysen, B., Virgo, D., and Seifert, F.A. (1985) Relationships between properties and structure of
590 aluminosilicate melts. American Mineralogist, 70, 88-105.
591 Nakamura, M. (1995) Residence time and crystallization history of nickeliferous olivine
592 phenocrysts from the northern Yatsugatake volcanoes, Central Japan: Application of a growth
593 and diffusion model in the system Mg-Fe-Ni. Journal of Volcanology and Geothermal
594 Research, 66, 81-100.
595 Norman, M.D., and Garcia, M.O. (1999) Primitive magmas and source characteristics of the
596 Hawaiian plume: Petrology and geochemistry of shield picrites. Earth and Planetary Science
597 Letters, 168, 27-44.

598 Parsons, B., and Sclater, J.G. (1977) An analysis of the variation of ocean floor bathymetry and
599 heat flow with age. Journal of Geophysical Research, 82, 803-827.
600 Pearce, T.H. (1984) The analysis of zoning in magmatic crystals with emphasis on olivine.
601 Contributions to Mineralogy and Petrology, 86, 149-154.
602 Petry, C., Chakraborty, S., and Palme, H. (2004) Experimental determination of Ni diffusion
603 coefficients in olivine and their dependence on temperature, composition, oxygen fugacity, and
604 crystallographic orientation. Geochimica et Cosmochimica Acta, 68, 4179-4188.
605 Pietruszka, A.J., and Garcia, M.O. (1999) A rapid fluctuation in the mantle source and melting
606 history of Kilauea volcano inferred from the geochemistry of its historical summit lavas (1790-
607 1982). Journal of Petrology, 40, 1321-1342.
608 Pietruszka, A.J., Heaton, D.E., Marske, J.P., and Garcia, M.O. (2015) Two magma bodies
609 beneath the summit of Kīlauea Volcano unveiled by isotopically distinct melt deliveries from
610 the mantle. Earth and Planetary Science Letters, 413, 90-100.
611 Poland, M.P., Miklius, A., and Montgomery-Brown, E.K. (2014) Magma supply, storage, and
612 transport at shield-stage Hawaiian volcanoes. In Characteristics of Hawaiian Volcanoes,
613 Poland, M.P., Takahashi, T.J., and Landowski, C.M. eds., U.S. Geological Survey Professional
614 Paper 1801, 179-234.
615 Powers, H.A. (1955) Composition and origin of basaltic magma of the Hawaiian Islands.
616 Geochimica et Cosmochimica Acta, 7, 77-107.
617 Putirka, K.D. (2008) Thermometers and barometers for volcanic systems. Reviews in
618 Mineralogy and Geochemistry, 69, 61-120.
619 Putirka, K., Ryerson, F.J., Perfit, J., and Ridley, W.I. (2011) Mineralogy and composition of the
620 oceanic mantle. Journal of Petrology, 52, 279-313.

621 Rhodes, J.M. (1995) The 1852 and 1868 Mauna Loa picrite eruptions: Clues to parental magma
622 compositions and the magmatic plumbing system. In Geophysical Monograph 92. Rhodes and
623 Lockwood, Eds., Mauna Loa Revealed: Structure, Composition, History, and Hazards, p. 241-
624 262. American Geophysical Union, Washington, D.C., USA.
625 Rhodes, J.M., and Hart, S.R. (1995) Episodic trace element and isotopic variations in historical
626 Mauna Loa lavas: Implications for magma and plume dynamics. In Geophysical Monograph
627 92. Rhodes and Lockwood, Eds., Mauna Loa Revealed: Structure, Composition, History, and
628 Hazards, p. 263-288. American Geophysical Union, Washington, D.C., USA.
629 Rhodes, J.M., Wenz, K.P., Neal, C.A., Sparks, J.W., and Lockwood, J.P. (1989) Geochemical
630 evidence for invasion of Kilauea's plumbing system by Mauna Loa magma. Nature, 337, 257-
631 260.
632 Rhodes, J.M., and Vollinger, M.J. (2005) Ferric/ferrous ratios in 1984 Mauna Loa lavas: a
633 contribution to understanding the oxidation state of Hawaiian magmas. Contributions to
634 Mineralogy and Petrology, 149, 666-674.
635 Rhodes, J.M., Huang, S., Frey, F.A., Pringle, M., and Xu, G. (2012) Compositional diversity of
636 Mauna Kea shield lavas recovered by the Hawaii Scientific Drilling Project: Inferences on
637 source lithology, magma supply, and the role of multiple volcanoes. Geochemistry Geophysics
638 Geosystems, 13, doi: 10.1029/2011GC003812.
639 Rhodes, J.M. (2015) Major-element and isotopic variations in Mauna Loa magmas over 600 ka:
640 Implications for magma generation and source lithology as Mauna Loa transits the Hawaiian
641 plume. In Geophysical Monograph 208. Carey, Cayol, Poland, and Weis, Eds., Hawaiian
642 Volcanoes: From Source to Surface, p. 59-78. American Geophysical Union, Washington,
643 D.C., USA.

644 Shamberger, P.J., and Garcia, M.O. (2007) Geochemical modeling of magma mixing and magma
645 reservoir volumes during early episodes and Kilauea volcano's Puu Oo eruption. Bulletin of
646 Volcanology, 69, 345-352.
647 Shea, T., Costa, F., Krimer, D., and Hammer, J.E. (2015) Accuracy of timescales retrieved from
648 diffusion modeling in olivine: A 3D perspective. American Mineralogist, 100, 2026-2042.
649 Shorttle, O., and Maclennan, J. (2011) Compositional trends of Icelandic basalts: Implications
650 for short-length scale lithological heterogeneity in mantle plumes. Geochemistry, Geophysics,
651 Geosystems, 12, doi:10.1029/2011/GC003748.
652 Sobolev, A.V., Hofmann, A.W., Sobolev, S.V., and Nikogosian, I.K. (2005) An olivine-free
653 mantle source of Hawaiian shield basalts. Nature, 434, 590-597.
654 Sobolev, A.V., Hofmann, A.W., Kuzmin, D.V., Yaxley, G.M., Arndt, N.T., Chung, S-L.,
655 Danyushevsky, L.V., Elliott, T., Frey, F.A., Garcia, M.O., Gurenko, A.A., Kamenetsky, V.S.,
656 Kerr, A.C., Krivolutskaya, N.A., Matvienkov, V.V., Nikogosian, I.K., Rocholl, A.,
657 Suschevskaya, N.M., and Teklay, M. (2007) Estimating the amount of recycled crust in sources
658 of mantle derived melts. Science, 316, 412-417.
659 Stolper, E., Sherman, S., Garcia, M.O., Baker, M., and Seaman, C. (2004) Glass in the submarine
660 section of the HSDP2 drill core, Hilo, Hawaii. Geochemistry, Geophysics, Geosystems, 5, doi:
661 10.10292003GC000553.
662 Takahashi, E., and Nakajima, K. (2002) Melting processes in the Hawaiian plume: An
663 experimental study. In Geophysical Monograph 128. Takahashi, Lipman, Garcia, Naka, and
664 Aramaki, Eds., Hawaiian Volcanoes: Deep Underwater Perspectives, p. 403-418, American
665 Geophysical Union, Washington, D.C., USA.

Thornber, C.R., Heliker, C., Sherrod, D.R., Kauahikaua, J.P., Miklius, A., Okubo, P.G., Trusdell, F.A., Budahn, J.R., Ridley, W.I., and Meeker, G.P. (2003) Kilauea east rift zone magmatism: An episode 54 perspective. Journal of Petrology, 44, 1525-1559.

Toplis, M.J. (2005) The thermodynamics of iron and magnesium partitioning between olivine and liquid: Criteria for assessing and predicting equilibrium in natural and experimental systems. Contributions to Mineralogy and Petrology, 149, 22-39.

Vinet, N., and Higgins, M.D. (2011) What can crystal size distributions and olivine compositions tell us about magma solidification processes inside Kilauea Iki lava lake, Hawaii? Journal of Volcanology and Geothermal Research, 208, 136-162.

Wang, Z., and Gaetani, G.A. (2008) Partitioning of Ni between olivine and siliceous eclogite partial melt: experimental constraints on the mantle source of Hawaiian basalts. Contributions to Mineralogy and Petrology, 56, 661-678.

Wright, T.L. (1971) Chemistry of Kilauea and Mauna Loa lavas in space and time. U.S. Geological Survey Professional Paper, 735, 40 p.

Wright, T.L., and Fiske, R.S. (1971) Origin of the differentiated and hybrid lavas of Kilauea volcano, Hawaii. Journal of Petrology, 12, 1-65.

Yang, H., Frey, F.A., Clague, D.A.. and Garcia, M.O. (1999) Mineral chemistry of submarine lavas from Hilo Ridge, Hawaii: implications for magmatic processes within Hawaiian rift zones. Contributions to Mineralogy and Petrology, 135, 355-372.

Yoder, H.S., and Tilley, CE (1962) Origin of basaltic magmas: An experimental study of natural and synthetic rock systems. Journal of Petrology, 3, 342-532.

687 Zhukova, I., O'Neill, H. StC., Cambell, I.H., and Kilburn, M.R. (2014) The effect of silica
688 activity on the diffusion of Ni and Co in olivine. Contributions to Mineralogy and Petrology,
689 168, 1028-1029.

690

This is a preprint, the final version is subject to change, of the American Mineralogist (MSA)
Cite as Authors (Year) Title. American Mineralogist, in press.
(DOI will not work until issue is live.) DOI: http://dx.doi.org/10.2138/am-2017-5763

Revision 1

691 **Table 1.** Representative modes for Kīlauea lavas (volume %), based on 300 (vesicle-free)
692 counts/sample. Phenocrysts (ph, >0.5 mm), microphenocrysts (mph, 0.1-0.5 mm), matrix (<0.1
693 mm).
694

Location[a]	Eruption Date	Whole-rock MgO (wt%)[b]	Olivine		Cpx		Plag		Matrix
			ph	mph	ph	mph	ph	mph	
U	13-Jun-69	9.43	-	2.3	-	-	-	-	97.7
S	Aug 1971	10.01	-	0.3	-	-	-	-	99.7
P[c]	16-Aug-83	7.77	2.7	1.0	-	0.7	-	*[d]	95.6
P[c]	7-Sep-83	7.94	3.0	0.3	-	-	-	-	96.7
P[c]	18-Oct-87	8.11	1.0	3.0	-	-	-	-	96.0
P	20-July-90	9.04	5.7	-	-	-	-	-	94.3
P	5-Oct-92	7.93	-	4.7	-	-	-	-	95.3
P	18-May-94	7.61	0.3	2.7	-	0.3	-	-	96.7
P	22-Aug-96	8.23	0.7	2.7	-	-	-	-	96.7
P	13-Feb-99	7.41	-	1.7	-	-	-	-	98.3
P	4-Aug-00	8.29	0.3	4.3	-	-	-	-	95.3
P	12-Mar-03	7.62	1.3	5.0	-	0.3	-	-	93.3
P	17-Jun-07	8.53	-	2.0	-	*	-	-	98.0
P	6-Mar-10	7.18	-	0.7	-	0.7	-	0.7	97.9

695 Note(s): [a]Locations – S: Summit, 1971A-2 from Garcia et al. (2003), U: Upper East Rift Zone (rift zoned eruptions
696 not including Pu‘u ‘Ō‘ō), this sample is from Mauna Ulu, P: Pu‘u ‘Ō‘ō eruption; [b] for bulk compositions see Greene
697 et al. (2013) and Garcia et al. (2003); [c] indicates samples with textural evidence of mixing (e.g. normal and reverse
698 zoning of olivine) [d] * denotes phases that were observed but not counted.

699 **Table 2.** Representative microprobe analyses for olivine from historical Kīlauea lavas. Oxides are in wt%. Full dataset can be found in
700 Supplementary Material.

Sample	SiO_2	FeO[a]	NiO	MnO	MgO	CaO	Total	Fo[b]	Sample	SiO_2	FeO[a]	NiO	MnO	MgO	CaO	Total	Fo[b]
13-Jun	40.05	13.55	0.32	-	45.65	0.20	99.8	85.7	**18-Oct**	39.47	16.25	0.21	0.228	43.76	0.22	100.1	82.8
1969[c]	39.86	13.49	0.32	-	45.56	0.20	99.4	85.8	**1987**	39.64	15.70	0.23	0.22	44.35	0.22	100.4	83.4
	39.71	13.95	0.30	-	45.28	0.21	99.4	85.3		39.42	17.10	0.20	0.24	43.14	0.23	100.3	81.8
	39.80	13.70	0.32	-	45.43	0.22	99.5	85.5		39.33	17.07	0.20	0.24	43.12	0.25	100.2	81.8
	39.77	13.60	0.32	-	45.56	0.22	99.5	85.7		39.28	17.22	0.20	0.24	43.12	0.25	100.3	81.7
	39.80	13.61	0.32	-	45.48	0.22	99.4	85.6		39.32	17.13	0.20	0.24	43.27	0.24	100.4	81.8
Aug	40.44	11.70	0.38	-	47.67	0.19	100.4	87.9		39.27	17.53	0.19	0.25	42.75	0.25	100.2	81.3
1971[d]	40.40	10.93	0.41	-	48.54	0.18	100.5	88.1		39.31	17.14	0.19	0.24	42.73	0.24	99.8	81.6
	40.45	11.53	0.40	-	47.97	0.18	100.5	88.8		40.06	13.63	0.29	0.19	45.62	0.21	100.0	85.6
	40.21	12.95	0.34	-	46.57	0.19	100.2	86.5	**20-Jul**	39.27	17.09	0.21	0.24	43.02	0.23	100.1	81.8
	40.29	11.96	0.40	-	46.57	0.19	100.2	86.5	**1990**	39.16	17.22	0.21	0.24	43.00	0.22	100.1	81.7
	40.12	13.20	0.31	-	46.08	0.20	99.9	86.2		39.15	17.23	0.20	0.24	43.03	0.22	100.1	81.7
	39.84	14.01	0.26	-	45.44	0.21	99.8	85.3		39.01	17.10	0.21	0.24	42.89	0.23	99.7	81.7
	40.02	13.32	0.30	-	45.94	0.21	99.8	86.0		39.08	17.15	0.20	0.24	42.79	0.24	99.7	81.7
	40.07	13.29	0.31	-	46.09	0.20	100.0	86.1		39.21	17.14	0.20	0.24	42.70	0.31	99.8	81.6
	40.01	13.66	0.30	-	45.58	0.21	99.8	85.6		39.17	17.25	0.21	0.24	43.02	0.21	100.1	81.6
	40.18	10.80	0.41	-	48.31	0.18	99.9	88.9		39.15	17.27	0.20	0.24	42.79	0.24	99.9	81.5
	40.22	10.79	0.41	-	48.43	0.19	100.0	88.9	**4-Aug**	39.14	17.17	0.19	0.23	43.33	0.23	100.3	81.8
7-Sep	39.42	13.69	0.33	0.19	45.55	0.21	99.4	85.6	**2000**	39.32	17.23	0.18	0.23	43.22	0.23	100.4	81.7
1983	39.61	14.43	0.29	0.19	45.54	0.23	100.3	84.9		39.29	17.39	0.18	0.24	43.14	0.24	100.5	81.6
	39.20	14.56	0.28	0.20	44.83	0.24	99.3	84.6		39.13	17.40	0.18	0.24	42.87	0.23	100.1	81.5
	39.45	15.24	0.32	0.20	44.84	0.24	100.3	84.0		39.07	17.41	0.17	0.24	42.75	0.24	99.9	81.4
	39.41	15.37	0.28	0.20	44.69	0.24	100.2	83.8		39.15	17.55	0.17	0.24	42.91	0.24	100.3	81.3
	39.31	15.52	0.30	0.20	44.43	0.23	100.0	83.6		39.16	17.58	0.18	0.24	42.89	0.24	100.3	81.3
	39.39	15.72	0.29	0.21	44.44	0.24	100.3	83.5		39.23	17.68	0.17	0.24	42.65	0.24	100.2	81.1
	39.08	16.19	0.27	0.22	43.64	0.22	99.7	82.8		38.64	18.75	0.16	0.25	41.87	0.26	99.9	79.9
	38.97	16.53	0.28	0.22	43.36	0.23	99.6	82.4	**6-Mar**	39.45	17.94	0.19	0.23	41.41	0.21	99.4	80.5
	39.18	16.94	0.25	0.22	43.35	0.25	100.2	82.0	**2010**	39.74	17.90	0.18	0.23	41.44	0.25	99.7	80.5
	39.09	17.27	0.26	0.22	43.25	0.24	100.3	81.7		39.68	18.04	0.17	0.23	41.40	0.27	99.8	80.4
	38.95	17.27	0.24	0.23	42.89	0.24	99.8	81.6		39.74	18.03	0.18	0.23	41.59	0.25	100.0	80.4
	39.19	17.34	0.25	0.22	43.19	0.23	100.4	81.6		39.56	18.02	0.17	0.23	41.34	0.25	99.6	80.4
	38.89	17.33	0.24	0.23	42.68	0.22	99.6	81.5		39.71	18.14	0.18	0.23	41.47	0.25	100.0	80.3
	38.83	17.72	0.23	0.24	42.35	0.21	99.6	81.0		39.72	18.25	0.17	0.24	41.26	0.26	99.9	80.1
	38.93	17.94	0.25	0.23	42.59	0.23	100.2	80.9		39.48	18.39	0.17	0.24	41.11	0.26	99.7	80.0
	38.81	17.93	0.23	0.24	42.16	0.22	99.6	80.7		39.34	19.27	0.15	0.25	39.97	0.30	99.3	78.7

701 Note(s): [a]FeO reported as total iron; [b]Fo (forsterite) = [Mg/(Mg+Fe) x 100]; [c]Mauna Ulu; [d]1971A-2 from Garcia et al. (2003).

This is a preprint, the final version is subject to change, of the American Mineralogist (MSA)
Cite as Authors (Year) Title. American Mineralogist, in press.
(DOI will not work until issue is live.) DOI: http://dx.doi.org/10.2138/am-2017-5763

Table 3. Parental melt compositions, calculated to be in equilibrium with Fo_{91} olivine, used in fractional crystallization models. NBO/T and $D_{Ni}^{ol/melt}$ are reported for Fo_{91} olivine compositions.

Oxide (wt%)	Lō'ihi[a]	Kilauea[b]	Mauna Kea[c] (Low-Si)	Mauna Kea[c] (High-Si)	Mauna Loa[d]	Ko'olau[e]
SiO_2	46.62	47.54	46.42	48.68	48.3	50.18
TiO_2	1.88	1.64	1.88	1.84	1.55	1.59
Al_2O_3	9.96	9.24	9.96	10.15	9.91	9.98
Cr_2O_3	0.20	0.20	0.20	0.20	0.20	0.05
FeO	11.50	11.43	11.50	10.50	10.92	10.87
MnO	0.16	0.16	0.16	0.16	0.17	0.13
MgO	19.21	19.73	19.14	17.25	18.01	17.60
CaO	8.66	7.64	8.16	8.52	7.47	6.23
Na_2O	1.69	1.57	1.71	1.67	1.55	1.97
K_2O	0.34	0.30	0.27	0.29	0.25	0.43
P_2O_5	0.14	0.16	0.15	0.15	0.16	0.20
NiO[f]	0.11 or 0.09	0.11 or 0.09	0.11 or 0.09	0.11 or 0.09	0.11 or 0.09	0.11 or 0.09
% ol. add.	9.7	-	5.6	4.0	1.9	6.7
NBO/T	1.66	1.61	1.61	1.45	1.45	1.36
$D_{Ni}^{ol/melt}$	4.3	4.25	4.25	4.0	4.0	3.8

Note(s): [a]Garcia et al. 1993; [b]Matzen et al. 2011, no olivine addition because parental composition as already in equilibrium with Fo_{91}; [c]Stolper et al. 2004; [d]Rhodes 2015; [e]Norman and Garcia 1999; [f]Imposed NiO concentration for all parental compositions (similar to Sobolev et al. 2005, Putirka et al. 2011).

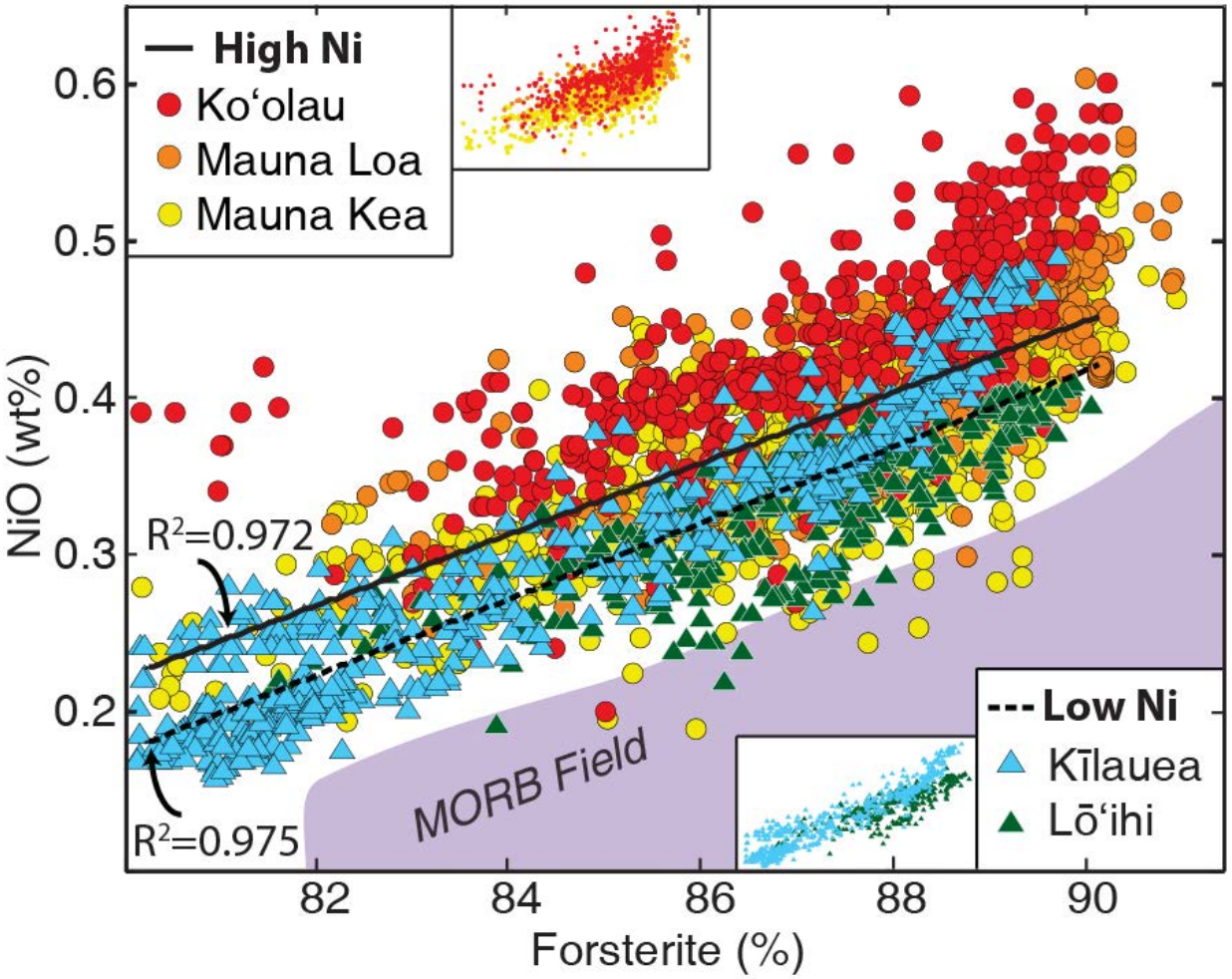

Figure 1. Forsterite (%) vs. NiO (wt%) for olivine from Ko'olau, Mauna Loa, Mauna Kea, Lō'ihi, and Kīlauea lavas. The data can be separated into high-Ni (warm colors) and low-Ni volcano groups (cool colors). Linear regressions for High- (solid line) and Low-Ni (dashed line) groups with R^2 values. Olivine from the high-Ni volcanoes have a wider range in NiO at a given Fo compared to the low-Ni volcanoes (inset figures). Ko'olau olivine are from Garcia (2002) and Sobolev et al. (2007), Mauna Loa, Mauna Kea, and Lō'ihi are from Sobolev et al. (2007). Kīlauea data are from this study and Sobolev et al. (2007). MORB field (purple) from Sobolev et al. (2007).

This is a preprint, the final version is subject to change, of the American Mineralogist (MSA)
Cite as Authors (Year) Title. American Mineralogist, in press.
(DOI will not work until issue is live.) DOI: http://dx.doi.org/10.2138/am-2017-5763

Revision 1

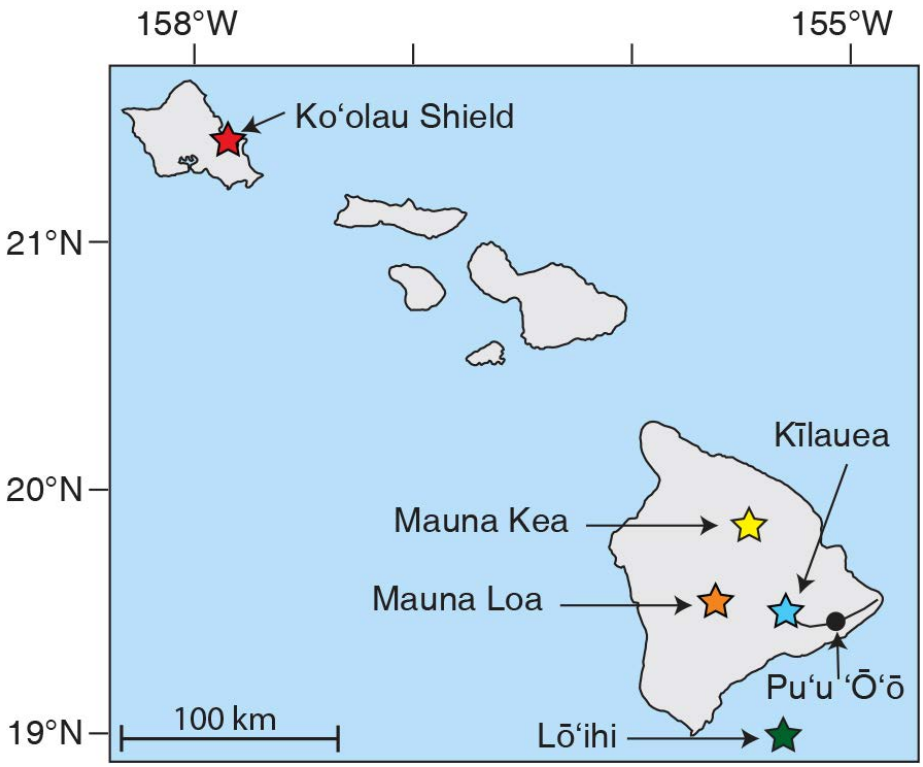

719

720 **Figure 2.** Map of the Hawaiian Islands showing the summit locations of the high-Ni (Koʻolau
721 Shield, Mauna Loa, and Mauna Kea) and low-Ni (Kīlauea and Lōʻihi) volcanoes. Stars indicate
722 the location of volcano summits, color coordinated to match Figure 1. The Puʻu ʻŌʻō eruption
723 (black dot) is located 20 km southeast of Kīlauea's summit along its East Rift Zone (curved line).

724

This is a preprint, the final version is subject to change, of the American Mineralogist (MSA)
Cite as Authors (Year) Title. American Mineralogist, in press.
(DOI will not work until issue is live.) DOI: http://dx.doi.org/10.2138/am-2017-5763

Revision 1

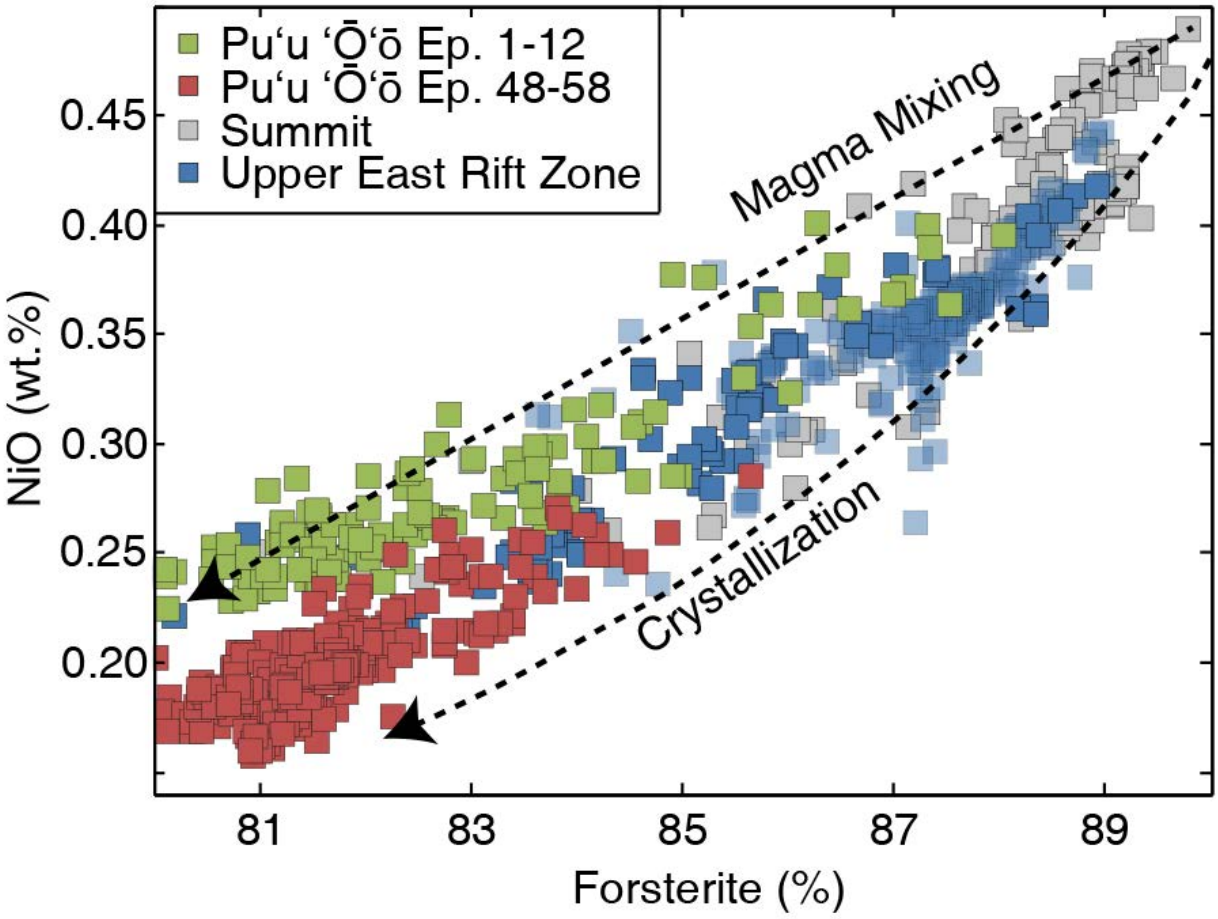

Figure 3. Forsterite (Fo%) vs. NiO (wt%) for Kīlauea olivine core compositions. Episode (Ep.) 1-12 (n=8 samples) Pu‘u ‘Ō‘ō olivine cover a period of magma mixing. Later Pu‘u ‘Ō‘ō Ep. 48-58 (n=31) olivine are from lavas that lack obvious petrographic signs of mixing. See Supplementary Data for specific samples and episodes. Vectors denote the evolution of olivine compositions during progressive crystallization and magma mixing (after Wang and Gaetani 2008). Upper ERZ includes historical rift zone eruptions (n=4), not including Pu‘u ‘Ō‘ō. Summit eruptions are from 1500-1971 (n=6). Light blue squares are data from Sobolev et al. 2007.

This is a preprint, the final version is subject to change, of the American Mineralogist (MSA)
Cite as Authors (Year) Title. American Mineralogist, in press.
(DOI will not work until issue is live.) DOI: http://dx.doi.org/10.2138/am-2017-5763

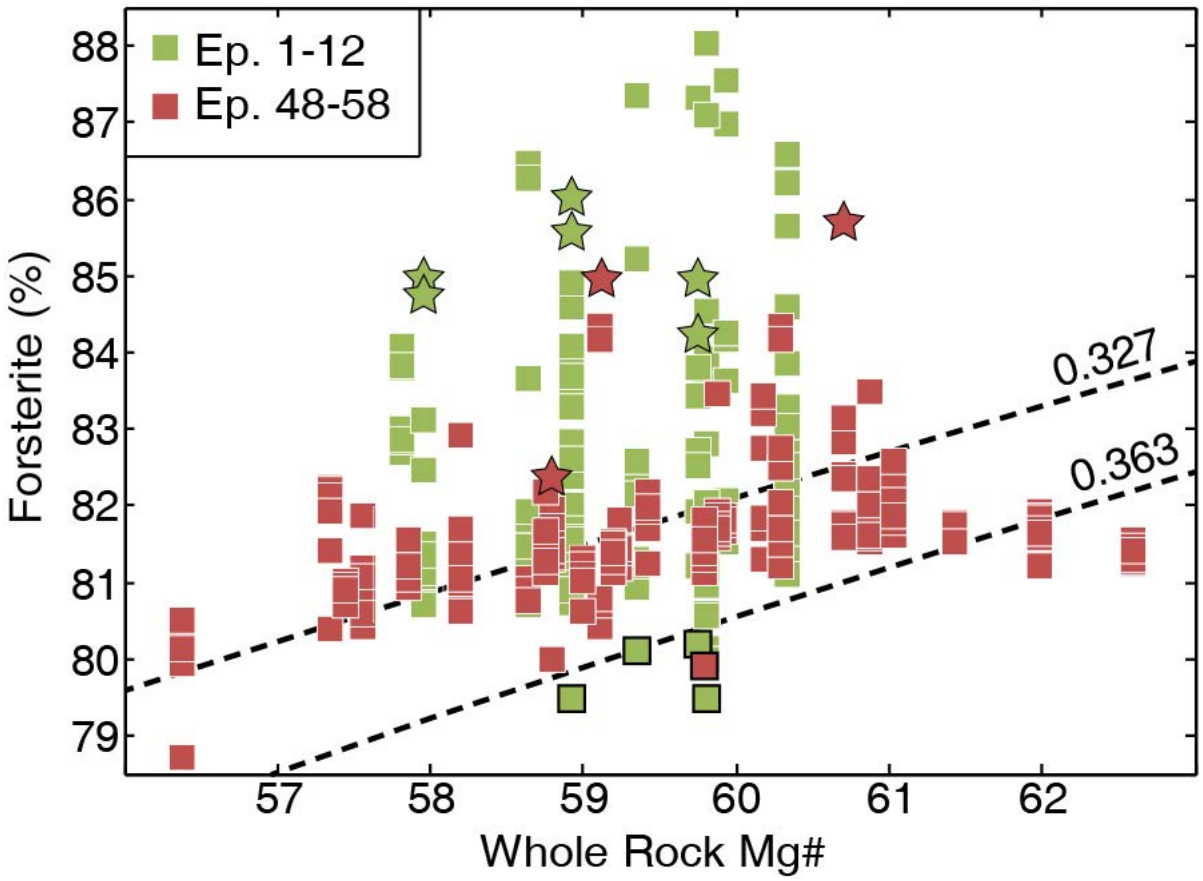

Figure 4. Representative whole-rock Mg-numbers [Mg/(Mg+Fe^{2+}) x 100] plotted against olivine core forsterite contents for Kīlauea lavas. The Mg-number is calculated assuming 90% of the total iron is Fe^{2+}, based on iron titration measurements of Kīlauea lavas (e.g. Moore and Ault 1965; Byers et al. 1985; Rhodes and Vollinger 2005). The dashed lines denote the shallow pressure (1 atm) equilibrium field for basaltic magma ($K_{d\ Fe/Mg}$ =0.345±0.018 at 2σ; Matzen et al. 2011). Higher Mg# samples (e.g. 62.0-62.5) that dominantly plot below the equilibrium field have probably experienced olivine accumulation, whereas samples above the field represent non-equilibrium olivines from mixed magmas or delayed fractionation. Stars indicate examples of olivine with decoupled Fo-NiO zoning profiles, whereas squares with black outlined boxes indicate core compositions of reversely zoned crystals. For each sample, 5-12 olivine crystals were analyzed (similar Fo contents appear stacked; see Supplementary Material for analyses).

This is a preprint, the final version is subject to change, of the American Mineralogist (MSA)
Cite as Authors (Year) Title. American Mineralogist, in press.
(DOI will not work until issue is live.) DOI: http://dx.doi.org/10.2138/am-2017-5763

Revision 1

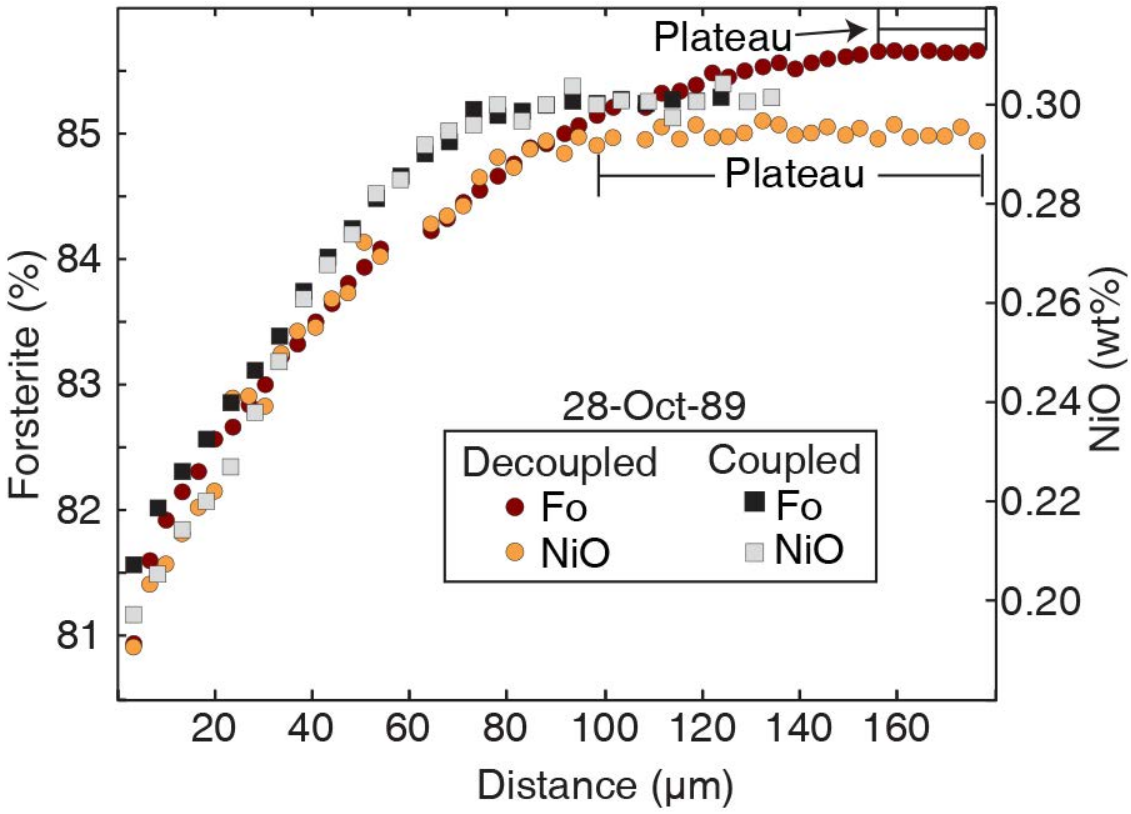

Figure 5. Examples of two Fo (%) and NiO (wt%) profiles from the same sample (28-Oct-89) that are similar in size and composition. Plateaus are regions where the composition (e.g. Fo or NiO) does not vary outside the analytical error. The sample name corresponds to the date it was collected during the Pu‘u ‘Ō‘ō eruption. Spot analyses with low totals due to cracks or spinel inclusions were removed and appear as gaps in otherwise regularly spaced analyses. Errors for all analyses are smaller than the symbol size.

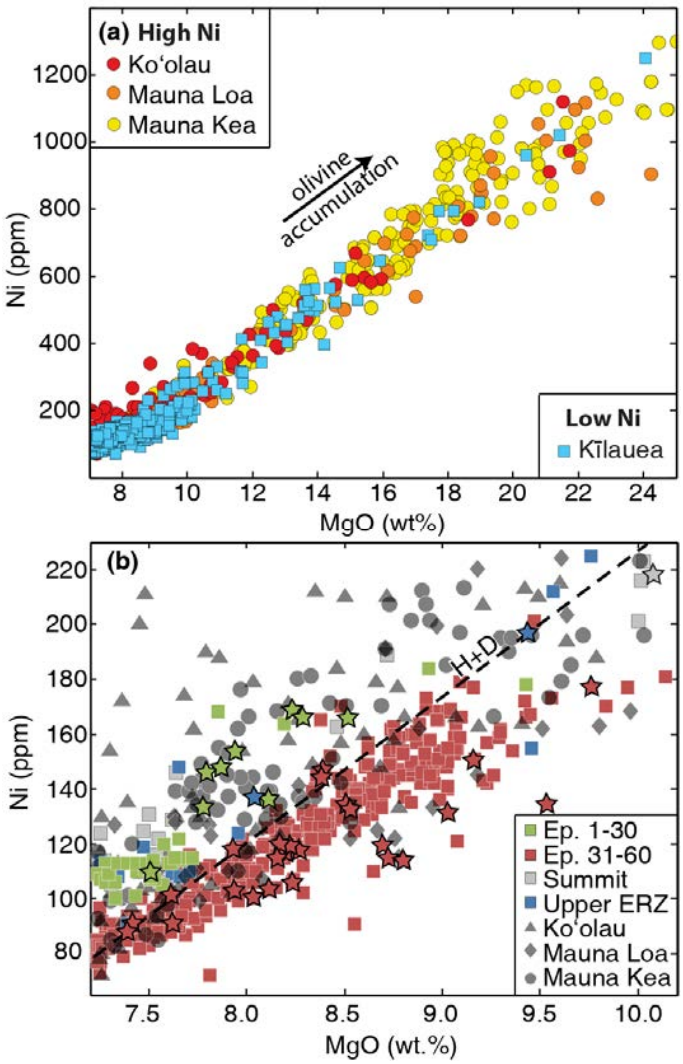

Figure 6. (a) Whole-rock MgO vs. Ni for Hawaiian volcanoes. All samples were analyzed in the same facility (University of Massachusetts) to avoid inter-laboratory differences. (b) Pu‘u ‘Ō‘ō samples are subdivided into early, mixed lavas from episodes (Ep.) 1-30 (Shamberger and Garcia 2007), and later unmixed samples (Ep. 31-60; minus Ep. 54). Dashed line (H+D) represents Kīlauea trend from Hart and Davis (1978). The line separates most early, mixed Ep. 1-30 Pu‘u ‘Ō‘ō lavas from later unmixed Ep. 31-60 lavas. Symbols with dark outlines indicate Kīlauea samples used for olivine analyses in this study. Data are from Pietruszka and Garcia 1999, Marske et al. 2007, Garcia et al. 2003, Greene et al. 2013, Marske et al. unpublished, and this study (Supplementary Data File 1) for Kīlauea, Rhodes 1995, Rhodes and Hart 1995 for Mauna Loa, Rhodes et al. 2012 for Mauna Kea, and Frey et al. 1994, Jackson et al. 1999, and Haskins and Garcia 2004 for Ko‘olau.

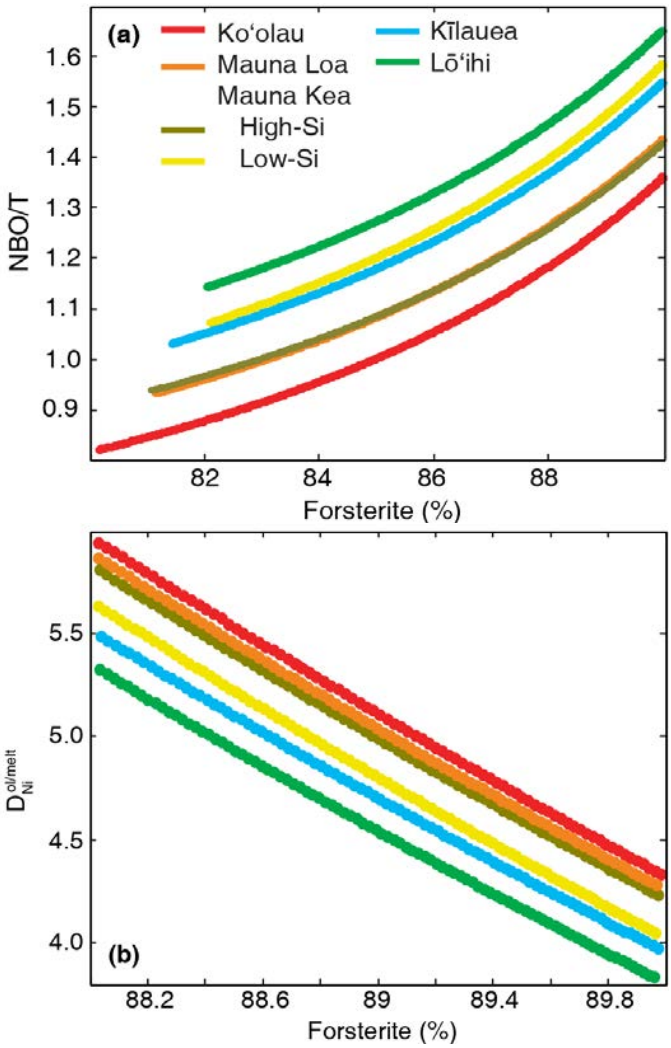

Figure 7. (a) NBO/T in standard fractional crystallization models of parental melt compositions for Ko'olau, Mauna Loa, Mauna Kea (high- and low- SiO_2), Kīlauea, and Lō'ihi starting at 1450 °C until ~35 vol.% olivine is crystallized (producing variable final % forsterite due to small variations in parental composition and $D_{Mg}^{ol/melt}$). (b) The changing $D_{Ni}^{ol/melt}$ from Wang and Gaetani 2008, which is sensitive to variations in NBO/T, along fractional crystallization trends for primitive olivine at each volcano.

This is a preprint, the final version is subject to change, of the American Mineralogist (MSA)
Cite as Authors (Year) Title. American Mineralogist, in press.
(DOI will not work until issue is live.) DOI: http://dx.doi.org/10.2138/am-2017-5763

Revision 1

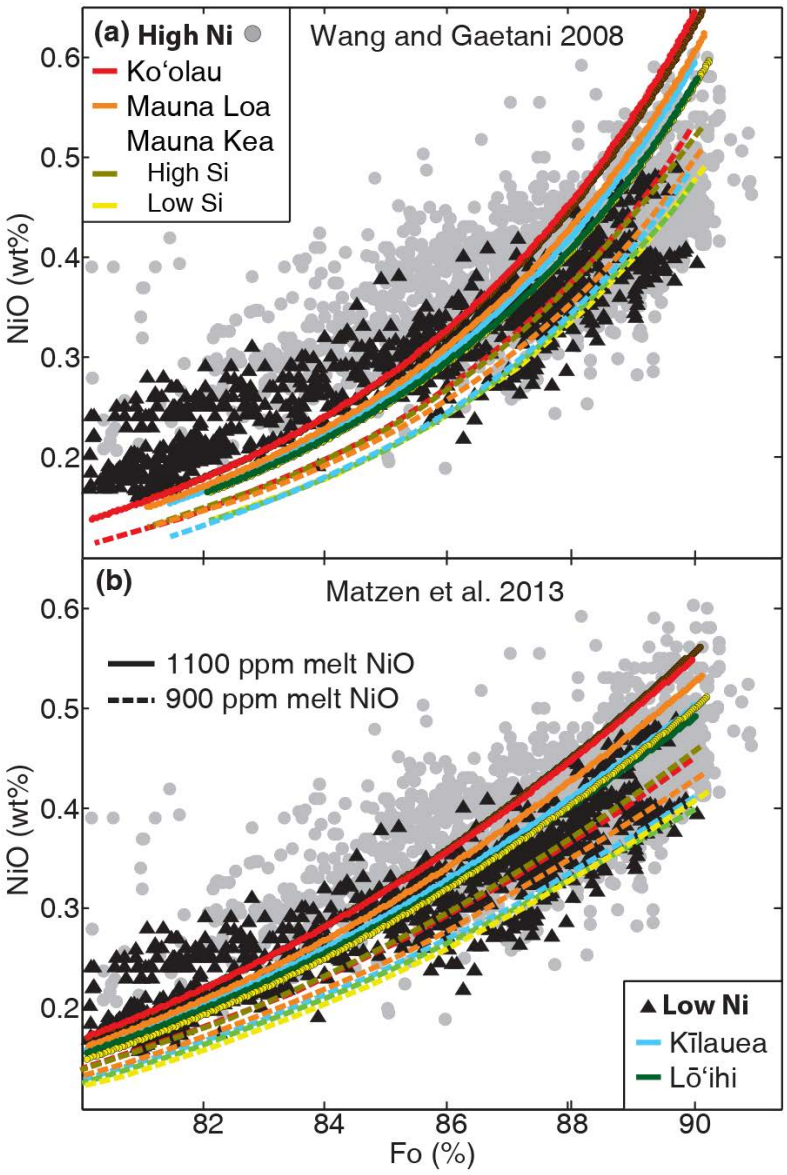

Figure 8: Olivine forsterite (%) vs. NiO (wt%) for fractional crystallization models at 1 GPa using (a) Wang and Gaetani (2008) and (b) Matzen et al. (2013) using parental melt compositions from Table 3. High- (grey) and low-Ni (black) volcano groups as in Fig. 1. Solid lines represent models run for parental melts with 0.11 wt% NiO; dashed lines for parental melts with 0.09 wt% NiO.

This is a preprint, the final version is subject to change, of the American Mineralogist (MSA)
Cite as Authors (Year) Title. American Mineralogist, in press.
(DOI will not work until issue is live.) DOI: http://dx.doi.org/10.2138/am-2017-5763

Revision 1

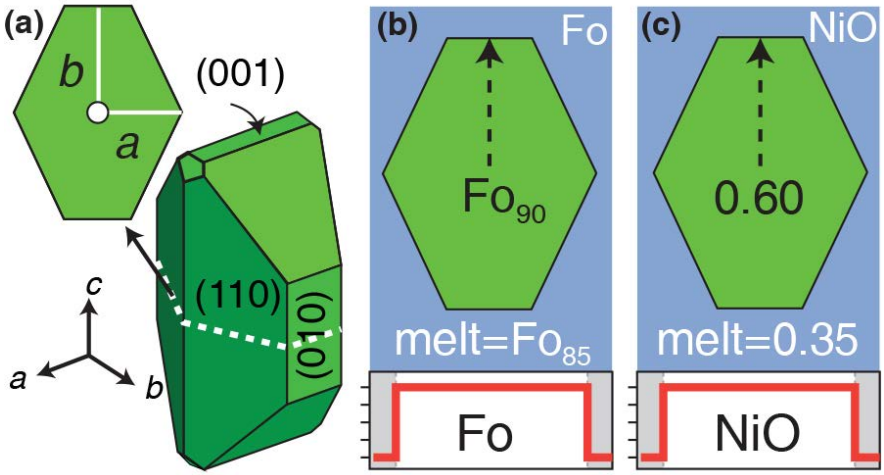

Figure 9: (a) 3D numerical olivine model showing 2D section (dashed white line) taken perpendicular to the c-axis [001]. (b and c) Initial crystal (black text) and melt (white text) compositions used in models. Melt forsterite is equivalent to a melt Mg# in equilibrium with Fo_{85} olivine. Melt and olivine NiO concentrations reported as wt%. Rim-to-rim concentration profile (bottom red lines) indicates sharp boundary between crystal and melt before diffusion has occurred. Black dashed line marks location of profile selection along [010] (b-axis) after diffusive re-equilibration with the surrounding melt.

This is a preprint, the final version is subject to change, of the American Mineralogist (MSA)
Cite as Authors (Year) Title. American Mineralogist, in press.
(DOI will not work until issue is live.) DOI: http://dx.doi.org/10.2138/am-2017-5763

Revision 1

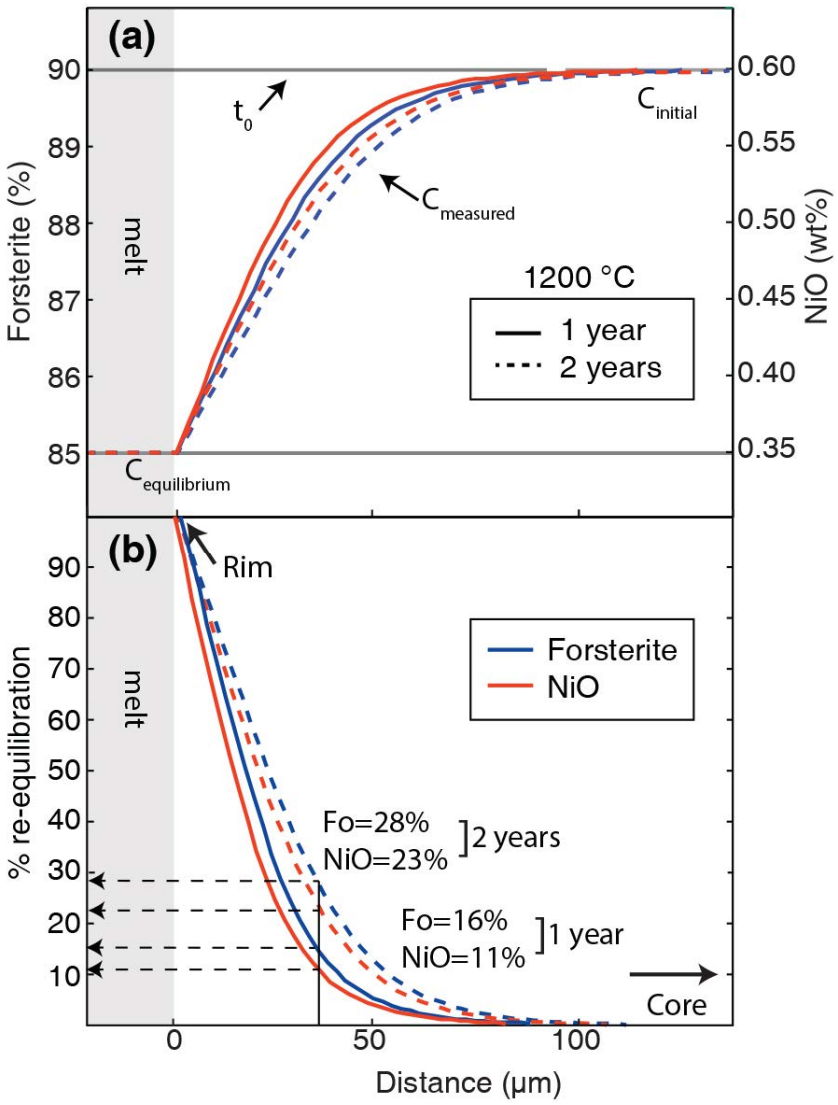

Figure 10: Results from numerical olivine diffusion models. (a) Forsterite (blue) and NiO (red) profiles along the b-axis in the olivine section. Solid line is one year of diffusion and dashed line is two years of diffusion. $C_{initial}$ and $C_{equilibrium}$ values labeled for starting crystal and surrounding melt compositions as in Fig. 8. (b) Results of % re-equilibration calculation (Eq. 1) using $C_{initial}$, $C_{equilibrium}$, and $C_{measured}$ (zoning profiles from *a*). In this ideal section through the crystal's center, the core retains $C_{initial}$ after diffusion has occurred.

801

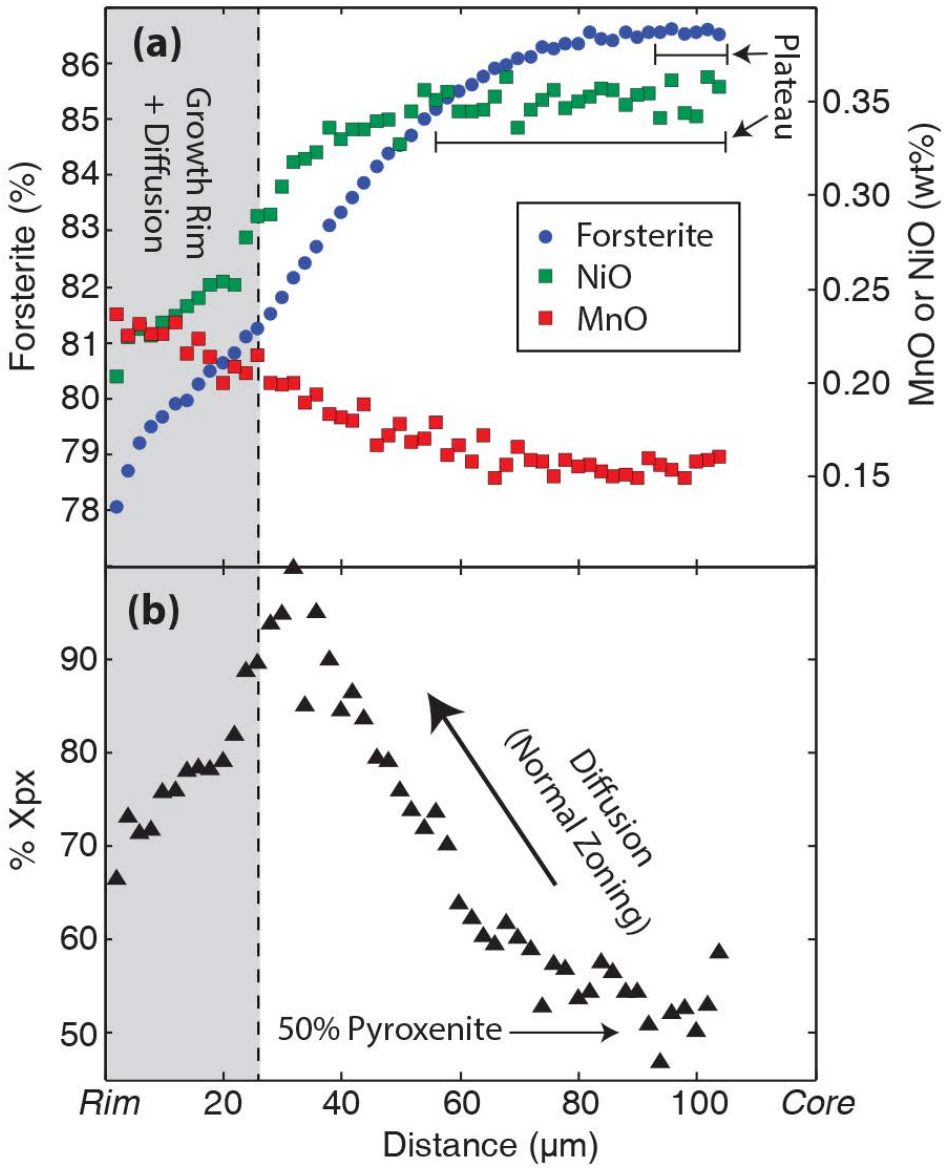

802

803 **Figure 11.** (a) Normally zoned and decoupled Kīlauea olivine (1670 C.E. summit lava flow)
804 with complex rim zoning influenced by growth and diffusion (evident in multiple changes in
805 slope for Fo; see Supplementary Data File 2 for analyses) and (b) calculated pyroxenite
806 (Gurenko et al. 2010) of the profile from the core plateau to the rim. Scatter in the % Xpx
807 calculated for the core region is due to analytical variability in minor elements (panel a).
808

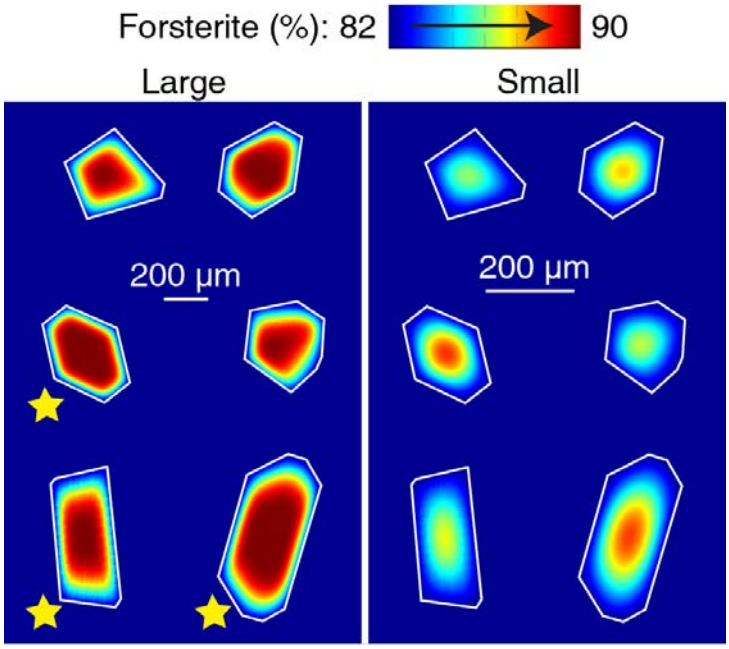

Figure 12. Examples of numerical "thin sections" for large (800 µm; left) and small (400 µm; right) olivine diffusion models (full dataset can be found in Supplementary Material). The small model was scaled up 2x to provide direct comparison with the large model. Thin white line marks the crystal margins within the melt (blue background). Yellow stars next to sections from the large model indicate preservation of initial compositions and recovery of original % Xpx values. Each section is either (1) near the crystal's core and/or (2) sectioned parallel or sub-parallel to the c-axis.